STRUCTURAL AND FUNCTIONAL ANALYSIS OF THE LIGAND BINDING POCKET OF BITTER TASTE RECEPTOR T2R4

by

Rohini Billakanti

A Thesis submitted to the Faculty of Graduate Studies of

The University of Manitoba

In partial fulfillment of the requirements of the degree of

MASTER OF SCIENCE

Faculty of Dentistry

Department of Oral Biology

University of Manitoba

Winnipeg

Canada

ABSTRACT

Bitter taste is one of the five basic taste modalities, and is mediated by 25 bitter taste receptors (T2Rs) in humans. How these few receptors recognize a wide range of structurally diverse bitter compounds is not known. To address this question, structural and functional studies on T2Rs are necessary. Quinine is a natural alkaloid and one of the most intense bitter tasting compounds. Previously it was shown that quinine activates T2R4, however, whether T2R4 has only one binding site for quinine, and the amino acids on the receptor involved in binding to quinine remain to be determined. In this study, the ligand binding pocket on T2R4 for quinine was characterized using a combination of approaches. These included molecular model guided site-directed mutagenesis, characterization of the expression of the mutants by flow cytometry, and functional characterization by cell based calcium imaging. Twelve mutations were made in T2R4 and their expression and function were characterized. Results show that the ligand binding pocket of T2R4 for quinine is situated on the extracellular side, and is formed by the residues present on the transmembrane regions TM3, TM4, and extracellular loop regions ECL2 and TM6-ECL3-TM7 interface. Further, this study identified the following amino acids : A90, F91, Y155 N173, T174, Y258 and K270 to play an important role in quinine binding to T2R4. The detailed study of residues interacting with ligand will help in understanding how various ligands interact with T2Rs, and facilitate the pharmacological characterization of potent antagonists or bitter taste blockers. The characterization of novel ligands, including bitter taste blockers will help in dissecting the signaling mechanism(s) of T2Rs, and help in the development of novel therapeutic tools for the food and drug industry.

ACKNOWLEDGEMENT

I thank my parents for their love and encouragement without whom my MSc in Canada would not have been possible.

I am very grateful to my supervisor Dr. Prashen Chelikani who gave me this wonderful opportunity to work in his lab. His expertise, invaluable guidance and patience have been my driving force to complete the thesis.

I thank my committee members Dr. Raj Bhullar and Dr. Hugo Bergen for their support. I appreciate my lab members Sai, Raja and others for their help in my project.

I am thankful to my friend Aarif for his help in finishing my thesis.

TABLE OF CONTENTS

ABSTRACT **ii**

ACKNOWLEDGEMENTS **iii**

TABLE OF CONTENTS **iv**

LIST OF TABLES **vii**

LIST OF FIGURES **viii**

LIST OF ABBREVIATIONS **x**

1. INTRODUCTION

1.1 Taste perception 1

1.1.2 Physiology of the taste system 1

1.1.3 Types of TRCs 2

1.1.4 Types of papillae 3

1.1.5 Types of taste modalities 3

1.1.6 Taste coding 8

1.1.7 Taste receptors 8

1.1.7.1 Sweet and umami taste receptors (T1Rs) 11

1.1.7.2 Bitter taste receptors (T2Rs) 11

1.1.8 Expression of T2Rs in oral tissue 13

1.1.9 Expression of T2Rs in extra-oral tissues 13

1.2 Tastants / Ligands 14

1.3 T2R signaling pathway 15

2. RATIONALE AND OBJECTIVES

2.1 Rationale 18

2.2 Specific objectives of this project 19

2.2. Specific objective 1 19

2.2.2 Specific objective 2 19

3. MATERIALS AND METHODS

3.1 Materials 20

3.2 Composition of buffers and media 21

3.3 Methods 21

3.3.1 Preparation of LB-ampicillin plates 21

3. 3.2 Wild type TAS2R4 and mutants 22

3. 3.3 Transformation of competent *E.Coli* 22

3. 3.4 Plasmid DNA extraction from *E.coli* 23

3. 3.4.1Isolation of plasmid DNA using QIAprep Spin 23

3. 3.4.2 Isolation of plasmid DNA using QIAGEN Maxiprep 25

3.3.5 Agarose gel electrophoresis 26

3.3.6 Preparation of glycerol stocks 26

3.3.7 Expression of TAS2R4 in Human Embryonic Kidney (HEK293T) cells 27

3.3.8 Calcium assay 27

3.3.9 Flow cytometry 28

3.3.10 Molecular modeling 29

3.3.11 Autodock Vina 30

3.3.12 T2R4 Mutants 30

4. RESULTS

4.1 DNA manipulation 33

4.2 Secondary structure and homology model of T2R4 33

4.3 Mutagenesis guided by molecular model of T2R4 34

4.4 Characterization of the expression of the WT-T2R4 and mutants 38

4.5 Functional characterization of the WT-T2R4 and mutants 38

5. DISCUSSION 55

5.1 TM3 mutants 56

5.2 TM4 mutant 57

5.3 ECL2 mutants 57

5.4 TM6-ECL3-TM7 mutants 58

5.5 Conclusion and future directions 59

6. REFERENCES 60

LIST OF TABLES

I.	Types of papillae	5
II.	Mean fluorescence intensity (MFI) of T2R4 and its mutants as determined by flow cytometry	39

LIST OF FIGURES

1. Taste receptor cells 4
2. Distribution of papillae on tongue 6
3. The five basic taste signal transduction pathways 9
4. Encoding of the taste qualities at the periphery 10
5. GPCR signaling pathways 12
6. Bitter taste signal transduction mechanism 17
7. pcDNA3.1inserted with TAS2R4 gene 24
8. Nucleic acid (DNA) and amino acid sequence of T2R4 32
9. Agarose gel electrophoresis of WT-TAS2R4 and its mutants 35
10. Models of the T2R4 and quinine 36
11. Molecular model of T2R4 bound to quinine 37
12. Cell surface expression of WT-T2R4 and its mutants 40
13. Concentration-dependent changes in intracellular calcium induced by quinine in HEK293T cells transiently transfected with T2R4 42
14. Concentration-dependent changes in intracellular calcium induced by quinine in HEK293T cells transiently transfected with A90G 43
15. Concentration-dependent changes in intracellular calcium induced by quinine in HEK293T cells transiently transfected with A90F 44
16. Concentration-dependent changes in intracellular calcium induced by quinine in HEK293T cells transiently transfected with F91A 45
17. Concentration-dependent changes in intracellular calcium induced by quinine in HEK293T cells transiently transfected with F92A 46

18. Concentration-dependent changes in intracellular calcium induced by quinine in HEK293T cells transiently transfected with Y155A 47
19. Concentration-dependent changes in intracellular calcium induced by quinine in HEK293T cells transiently transfected with N173A 48
20. Concentration-dependent changes in intracellular calcium induced by quinine in HEK293T cells transiently transfected with N173Q 49
21. Concentration-dependent changes in intracellular calcium induced by quinine in HEK293T cells transiently transfected with T174A 50
22. Concentration-dependent changes in intracellular calcium induced by quinine in HEK293T cells transiently transfected with T174S 51
23. Concentration-dependent changes in intracellular calcium induced by quinine in HEK293T cells transiently transfected with Y258A 52
24. Concentration-dependent changes in intracellular calcium induced by quinine in HEK293T cells transiently transfected with K270A 53
25. Concentration-dependent changes in intracellular calcium induced by quinine in HEK293T cells transiently transfected with K270R 54

ABBREVIATIONS LIST

A_{260}	Absorbance at 260 nm
A_{280}	Absorbance at 280 nm
Ca^{2+}	Calcium ion
cAMP	Cyclic adenosine monophosphate
DAG	Diacylglycerol
ECL	Extracellular loop
ER	Endoplasmic reticulum
FACS	Fluorescence-activated cell sorting
FBS	Fetal bovine serum
GDP	Guanosine 5'-diphosphate
GTP	Guanosine 5'-triphosphate
GPCR	G-protein coupled receptor
HEK	Human embryo kidney
ICL	Intracellular loop
IP_3	Inositol triphosphate
IP_3R	Inositol triphosphate receptor
Na^+	Sodium ion
PDE	Phosphodiesterase
TRC	Taste receptor cell
T2R	Bitter taste receptor
TM	Transmembrane
WT	Wild type

LIST OF COPYRIGHT MATERIALS

1. **Nature Publishing Group:** Chandrashekar, J., Hoon, M.A., Ryba, N.J.P., and Zuker, C.S. (2006). The receptors and cells for mammalian taste [Nature 444 (7117), 288-294].

    a. Figure 1. Taste-receptor cells

    b. Figure 4. Encoding of taste qualities at the periphery

CHAPTER ONE

INTRODUCTION

1.1 Taste perception

Animals consume food to get nutrients for their survival. However ingestion of poisonous substances can be life threatening. Taste or gustation is an important chemosensory perception which helps in analyzing the nutritive value and/or toxic nature of food consumed. Taste in mammals is mediated primarily through taste buds which are small anatomical structures present on the tongue, and are innervated by vagal (X), facial (VII) and glossopharyngeal nerves (IX) (Northcutt 2004). The activation of the nervous system, by the interaction of chemicals with particular taste receptors in the taste buds, leads to the experience of a given taste perception. Taste centers of the cortex in brain also play prominent roles in processing the sensory input. Gustation along with olfaction plays a crucial role in locating and identifying food. In humans, gustation contributes to the pleasure and enjoyment of a meal. Thus, taste has a prominent role in daily life.

1.1.2 Physiology of the taste system

Taste sensation acts as a gatekeeper to detect the nutritional value of the substances that humans consume. Substances which are useful for humans, such as high calorie foods containing carbohydrates, usually taste good and those which are harmful usually taste bitter, rendering us to differentiate important dietary substances. Taste receptor cells (TRCs) are specialized small epithelial cells that send a thin dendritic process to the epithelium of oral cavity to mediate the taste sensation (Katz et al. 2000). The turnover rate of TRCs is very rapid with a life span of 10 days (Beidler and Smallman 1965). About 100 TRCs are clustered in groups within the taste buds. These taste buds are distributed on tongue, pharynx and palate. Approximately, 10,000 taste buds are mounted on special folds and

protrusions on the epithelial surface of tongue known as papillae (Pfaffmann 1959). Taste sensation is initiated by the encounter of tastants or external stimuli with the taste receptors or proteins located in the microvilli on the apical surface of the TRCs. The taste signal transduction proteins include ion channels, G protein-coupled receptors (GPCRs), ligand-gated channels and transducing enzymes.

1.1.3 Types of TRCs

TRCs have been classified into four types based on their morphological differences in synaptic connectivity, cytoplasmic translucency and structure (Figure 1). They include :-

a) Type I or Dark cells

These cells have dark colored cytoplasm consisting of long microvilli on their apical surfaces. Lawton et al., have shown that the lamellate processes of these cells extend around other taste cells and express GLAST, a glial glutamate transporter, indicating glial function for these cells. This includes uptake of glutamate after its release at synapses (transmitter clearance) in taste buds (Lawton et al. 2000).

b) Type II or Light cells

In contrast to dark cells, light cells have light colored cytoplasm with short microvilli located on their apical surfaces. They are referred to as TRCs as they express all transducing elements of bitter, sweet and umami tastes (Hoon et al. 1999).

c) Type III or Intermediate cells

The cytoplasm of these cells is of intermediate color and these cells have significant synaptic contacts with gustatory nerve fibres. They express neural cell adhesion molecule (NCAM) (Nelson G. M. and Finger 1993) and synaptic membrane protein (SNAP25) (Yang et al. 2000).

d) Type IV or Basal cells:

While types I to III cells are elongated in structure, type IV are small disc like cells present at the base of the taste buds, referred to as basal cells. They are in constant touch with afferent nerve fibres.

1.1.4 Types of papillae

In mammals, due to the rough and irregular surface created by papillae; bacteria, cellular and food debris are trapped on the tongue which leads to the formation of an oral biofilm. Papillae are present in the oral cavity as well as the gustatory tissues like first one-third of esophagus, soft palate, larynx, pharynx, uvula and epiglottis (Table 1 and Figure 2).

1.1.5 Types of taste modalities

Humans perceive five basic taste modalities including salt, sour, sweet, bitter and umami (Figure 3). The specific properties of these basic taste modalities are described below.

(a) Bitter

As toxins, venoms and many plant alkaloids are bitter, vertebrates developed an instinctive antipathy to bitter modality. This feature helps in protecting the animal against consumption of noxious substances. However, bitter taste does not always provoke aversion as seen in case of coffee, broccoli, bitter olives, beer and dark chocolate. Bitter taste modality has evolved to protect animals from compounds having diverse chemical structures (Beauchamp 1995). This taste modality is mediated by cell surface receptors known as bitter taste receptors (T2Rs) that belong to the G protein-coupled receptors (GPCR) superfamily (Chandrashekar et al. 2000, Wong et al. 1996).

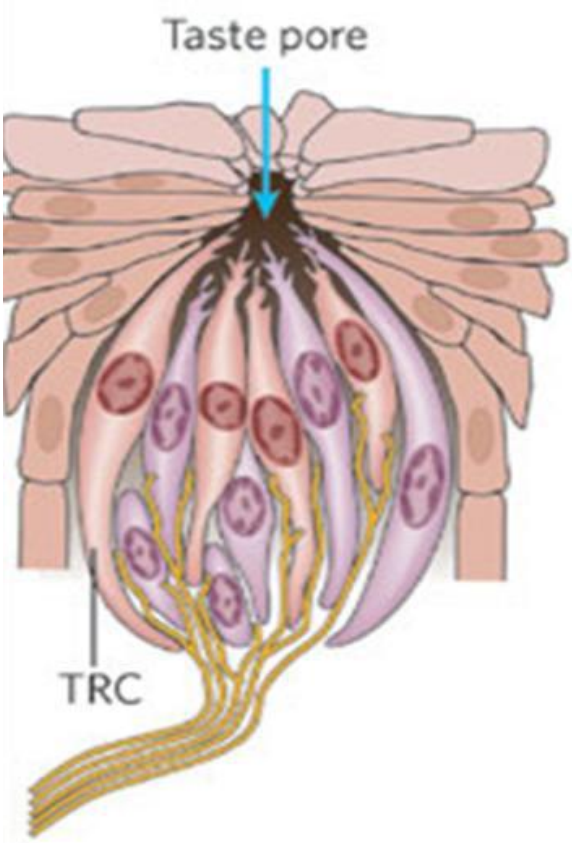

Figure 1. Illustration of a human taste bud
Taste bud showing the taste receptor cells and taste pore. Human taste buds are composed of 50-150 taste receptor cells (TRC), distributed across different papillae. TRCs project microvillae to the apical surface of the taste bud, where they form the taste pore, which is the site of interaction with the tastants.

Used with permission from Nature publishing group: Chandrashekar, J., Hoon, M.A., Ryba, N.J.P., and Zuker, C.S. (2006). The receptors and cells for mammalian taste [Nature 444 (7117), 288-294].

Table 1: Types of papillae
Papillae are broadly classified on the basis of their location and morphology. Human tongue consists of three types of papillae (Mbiene et al. 1997).

NAME	**Circumvallate**	**Foliate**	**Fungiform**
LOCATION ON TONGUE	Dorsal and Posterior	Posterior lateral edge	Anterior 2/3rds
MORPHOLOGY	Pin cushions	Ridges and grooves	Mushroom shaped
INNERVATIONS	Glossopharyngeal nerve	Glossopharyngeal and facial nerves	Facial nerve
NUMBER OF TASTE BUDS	100-1000	12-100	1-18

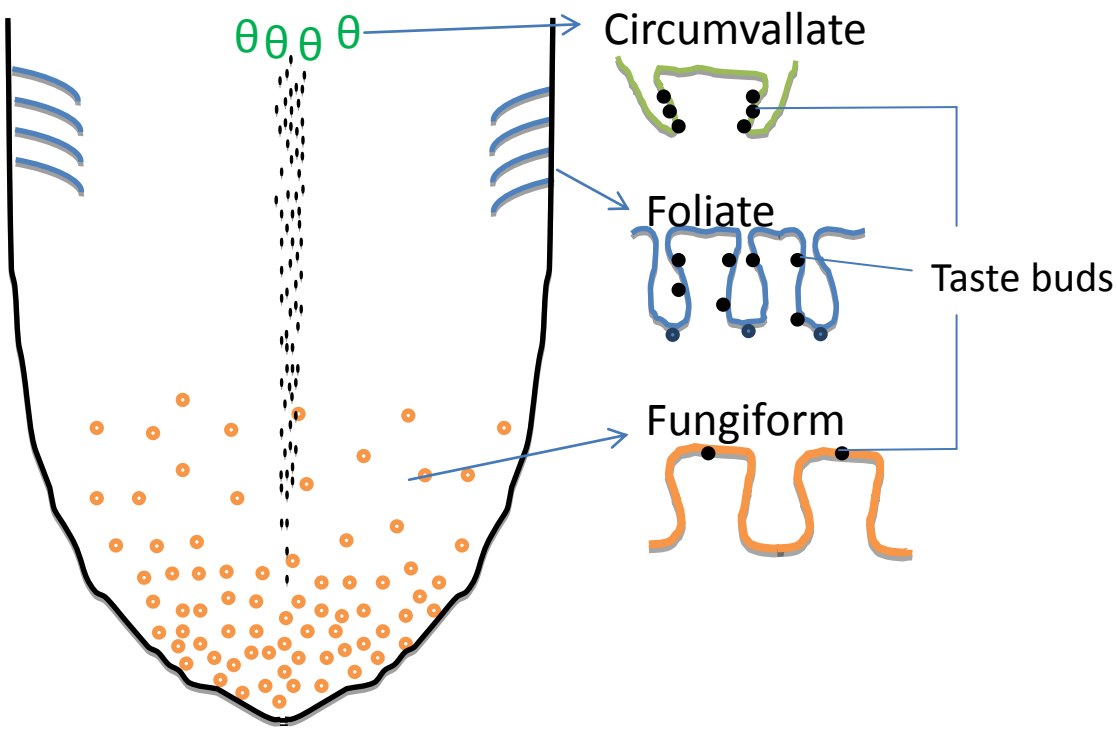

Figure 2. Distribution of papillae on tongue
Human tongue consists of three types of gustatory papillae. Circumvallate papillae are localized on the back of the tongue, foliate are on the posterior lateral edges and fungiform are situated in the anterior two-thirds. Papillae have taste buds mounted on them which in turn consist of TRCs. Circumvallate papillae have a higher number of taste buds, foliate have fewer and fungiform consist of very few taste buds.

(b) Umami

The term Umami was derived from Japanese word umai, which means delicious. This modality detects the taste of food containing amino acids such as L-aspartate and monosodium glutamate (Li et al. 2002). This quality was ingeniously used in food industry to enhance the flavour of food. Meat broth, ageing food, cheese and meat extracts have this taste (Lindemann 2001). Umami taste is mediated by a GPCR heterodimer of T1R1 and T1R3 (Li et al. 2002, Nelson G. et al. 2002).

(c) Sweet

Sweetness is elicited by soluble carbohydrates which are high calorie nutrients (Lindemann 2001). Sweetness which is produced by sugars evokes strong pleasantness (Ganchrow 1983). Glycosides and amino acids such as glycine, serine and alanine are sweet in nature (Zhang et al. 2003). This taste modality is mediated by a GPCR heterodimer of T1R2 and T1R3 (Li et al. 2002, Nelson G. et al. 2001).

(d) Sour

Sour taste is acceptable when weak but very aversive in strong doses. This modality aids in recognition of the presence of acids in food. It detects spoiled food, unripe fruits, helps in avoiding tissue damage and problems of acid-base regulation (Lindemann 2001). Acidic pH prevents bacterial growth (Gilbertson et al. 1992). Sour taste is sensed by transient receptor potential (TRP) channels. Polycystic kidney disease-1-like 3 (PKD1L3)/polycystic kidney disease-2-like 1(PKD2L1) are the two TRP channels that form heterodimers and possibly mediate sour sensation (Ishimaru and Matsunami 2009, Ishimaru et al. 2006).

(e) Salt

Salt taste is elicited by the presence of ions especially sodium and is involved in maintaining ion and water homeostasis. Table salt is the prototypical example for salty taste (Lindemann 2001). This taste is sensed by ion channel that allows direct entry of Na^+ ions

into the cell. Epithelial sodium channel (ENaC) a membrane-bound ion-channel was found to be selective to Na^+ ions (Palmer 1987).

1.1.6 Taste coding

To elucidate how taste is coded, two models, labeled line (Erickson 2000, Smith and St John 1999) and across-fibre (Caicedo et al. 2002, Smith et al. 2000) were proposed (Figure 4). Labeled line theory states that individual TRC responds to single taste modality and is innervated by exclusively tuned nerve fibre (Smith and St John 1999). Across-fibre model indicates that each TRC responds to multiple taste modalities and the same nerve fibre relays information for several taste qualities (Smith et al. 2000). There is also another possibility that each TRC responds to individual taste modality, however, the same nerve fibre relays information for multiple taste qualities.

1.1.7 Taste receptors

The initiation of taste signal transduction is triggered by the interaction of tastants or ligands with the proteins located on the cell membrane of TRCs. Among the five basic modalities sensed by the humans, bitter, sweet and umami tastes are transduced by GPCRs which are cell surface receptors. In contrast, salt and sour tastes are sensed by ion and/or transient receptor potential (TRP) channels (Ishimaru and Matsunami 2009, Ishimaru et al. 2006, Palmer 1987).

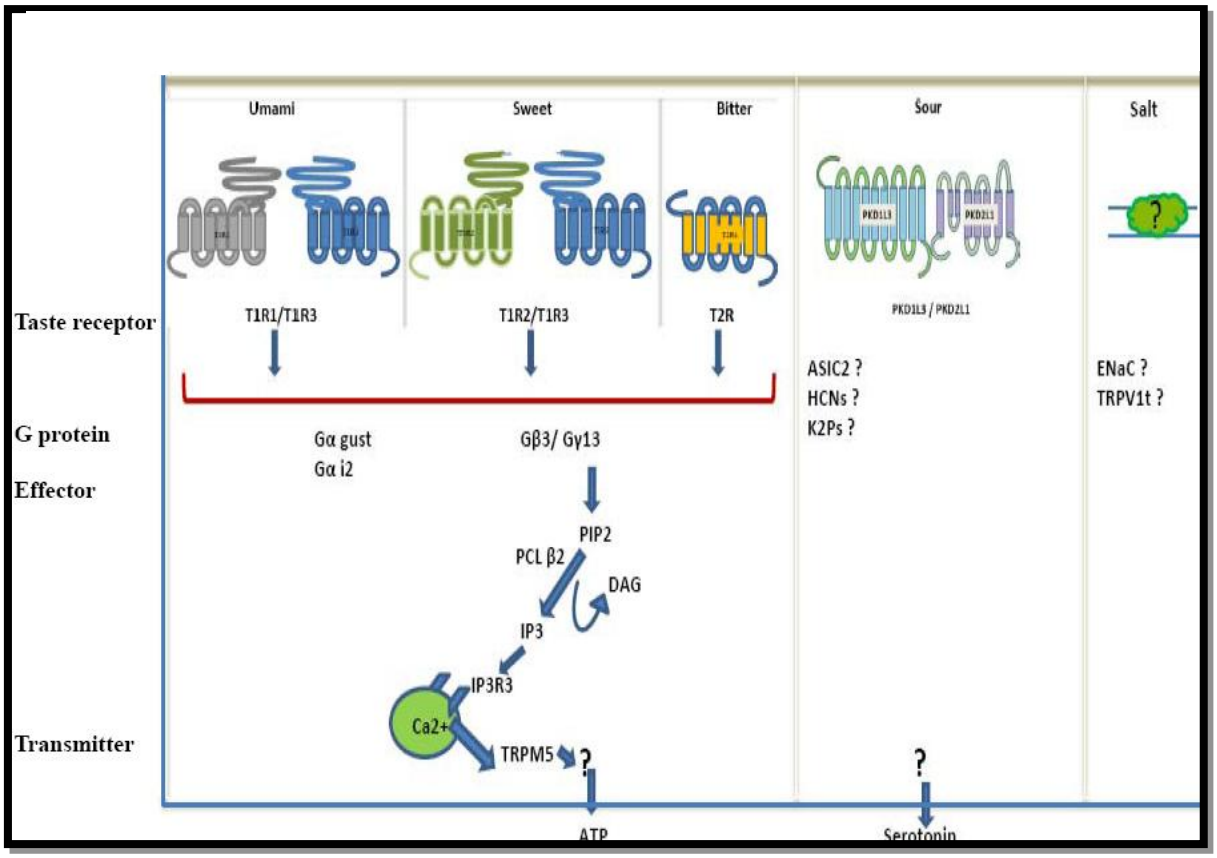

Figure 3. **The five basic taste signal transduction pathways**
Molecules involved in signaling pathway of five basic taste modalities. Type II taste cells express T1Rs and T2Rs, which belong to two distinct GPCR families. These are involved in recognition of umami, sweet and bitter ligands. G-proteins, PLCβ2, IP3 receptor and TRPM5 are the downstream signaling units which lead to neurotransmitter i.e., ATP release. TRCs also express PKD1L3/PKD2L1 heteromers which were suggested to be involved in transduction of sour taste. Serotonin may be the neurotransmitter involved in transmitting information to brain.

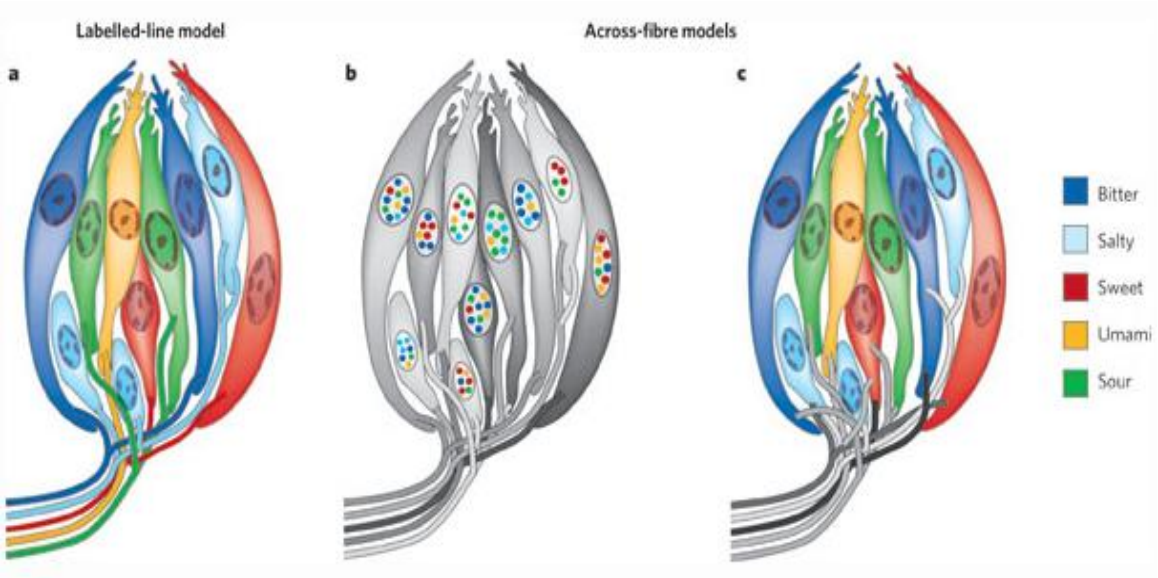

Figure 4. Encoding of the taste qualities at the periphery
(a) Labelled-line model, which states that receptor cells are tuned to respond to single taste modality – sweet, bitter, sour, salty or umami- and are innervated by the individually tuned nerve fibres. **(b, c)** Two contrasting models of across-fibre pattern. Either individual TRCs are tuned to multiple taste modalities and the same afferent fibre carries information for more than one taste modality (b), or TRCs are tuned to single modality but same afferent fibre carries information for more than one taste modality (c).

GPCRs are integral membrane proteins that have seven transmembrane helices (TM1-TM7), three extracellular loops (ECLs) and three intracellular loops (ICLs). The amino terminus is on the extracellular side, whereas the carboxyl terminus is on the intracellular side of the receptor. Approximately 80% of the neurotransmitters and hormones activate cellular signaling pathways by triggering GPCRs (Birnbaumer et al. 1990). Binding of a ligand on the extracellular side of the GPCR, leads to conformational changes in the receptor followed by the coupling of heterotrimeric G-proteins present on the intracellular side. This stimulates a series of intracellular signalling pathways (Figure 5) (Kroeze et al. 2003).

1.1.7.1 Sweet and Umami taste receptors (T1Rs)

T1Rs are reported to mediate the sensations of sweet and umami tastes. T1Rs consist of three receptors, T1R1, T1R2, T1R3 that belong to class C of the GPCR superfamily (Pin et al. 2003). A heterodimer of T1R1 and T1R3 functions as the umami receptor, while the heterodimer of T1R2 and T1R3 code for sweet taste (Bachmanov AA 2007). Like typical class C GPCRs, T1Rs have a large extracellular N-terminal domain referred to as the venus fly trap domain. The ligands bind to this venus fly trap domain in T1Rs and is the orthosteric binding site. T1Rs are reported to have an allosteric binding site (Gasparini et al. 2002).

1.1.7.2 Bitter taste receptors (T2Rs)

Bitter taste receptors or T2Rs, are known to detect harmful food substances before being swallowed. T2Rs belong to the GPCR superfamily (Wong et al. 1996). However, they

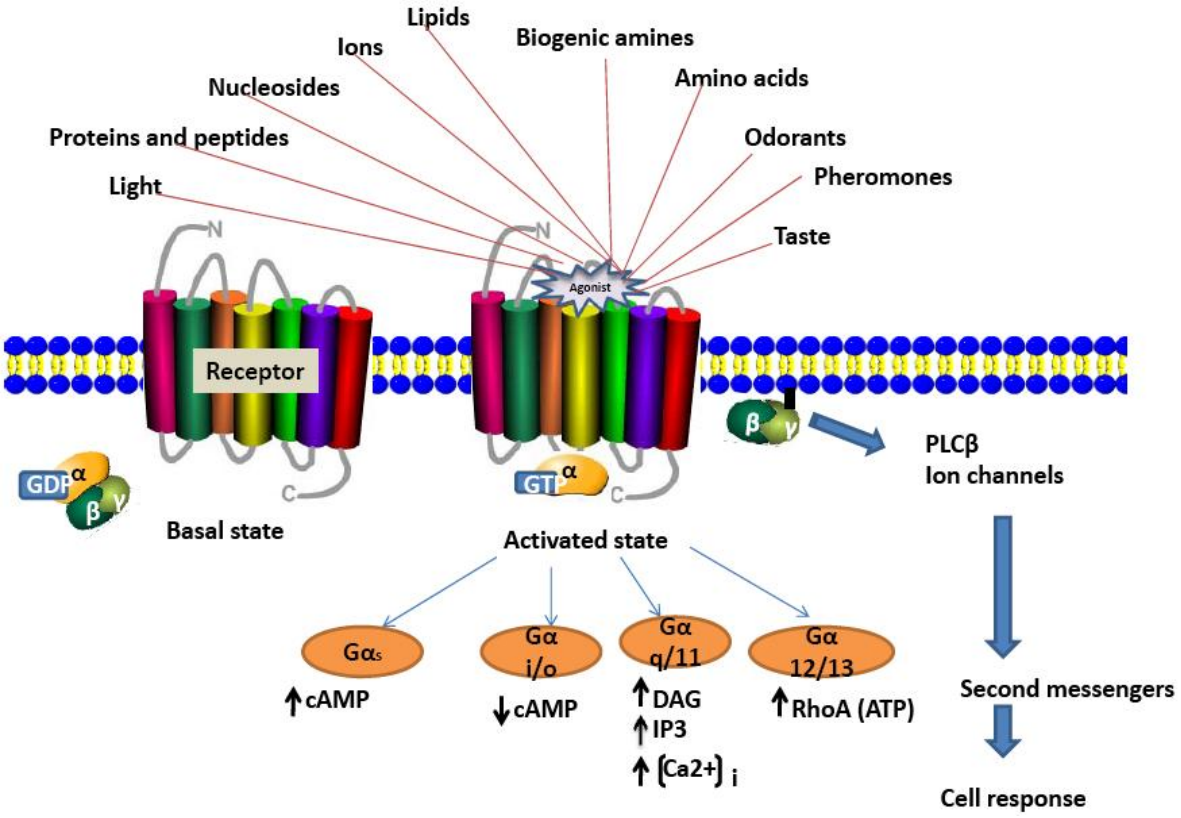

Figure 5. GPCR signaling pathways

Amino acids and ions, biogenic amines, lipids, peptides, proteins, others such as light, nucleotides and odorants activate GPCRs. GPCRs consist of 7 TMs, 3 ECLs and 3 ICLs. GPCRs couple predominantly to heterotrimeric G-proteins situated on the intracellular side. G-protein consists of α, β and γ subunits. The α-subunit is divided into 4 subfamilies namely- $G\alpha_s$, $G\alpha_i$, $G\alpha_q$ and $G\alpha_{12}$. The α-subunit interacts with the GPCR and the βγ subunits are predominantly membrane bound. In inactive state, the α-subunit is in the GDP bound state. Ligand binding leads to the conformational changes in receptor and dissociation of α and βγ subunits. The GDP attached to the α-subunit gets replaced with GTP and stimulates effector molecules which lead to activation of transcription factors following gene expression and biological responses.

are not grouped with any of the major classes of the GPCR superfamily (Pydi S. et al. 2014). T2Rs are encoded by intronless genes which are referred to as TAS2Rs. The Human Genome Organization (HUGO) gene nomenclature of TAS2R is used wherever the gene is mentioned (http://www.genenames.org/genefamilies/TASNR#TAS2R). Thus far, 25 TAS2Rs were found to be encoded by human genome (Adler et al. 2000). These genes are localized as clusters on chromosomes 5p15, 7q31, and 12p13 (Conte et al. 2002, Lagerstrom and Schioth 2008, Shi et al. 2003). These T2Rs consist of seven TMs, a short extracellular N-terminus, three ICLs, three ECLs and a short cytoplasmic C-terminus (Chandrashekar et al. 2000). Each T2R ranges between 290-330 amino acids in length (Conte et al. 2002, 2003). The 25 T2Rs have some conserved sequence motifs such as FlxxVN in TM1, LxxSR in TM2, LxxFY in TM3, LxxSL in TM5, HxxILI in TM7, and KIA, FxxLK in ICL2 (Kim et al. 2004, Maehashi and Huang 2009, Singh et al. 2011b).

1.1.8 Expression of T2Rs in oral tissue

In the oral cavity, taste buds of palate, circumvallate and foliate papillae consist of TRCs which selectively express TAS2R genes (Adler et al. 2000). Data obtained from *in situ* hybridization by Adler *et al.* suggested that "a single taste receptor cell expresses a large repertoire of T2Rs, suggesting that each cell may be capable of recognizing multiple tastants" (Adler et al. 2000). This supports the across-fibre model of taste coding.

1.1.9 Expression of T2Rs in extra-oral tissues

In addition to the oral cavity, T2Rs are also present in extra-oral tissues such as chemosensory cells of nasal epithelium (Finger et al. 2003), brain (Chen et al. 2011, Singh et al. 2011a), gastrointestinal neuroendocrine cells of the large intestine (Wu et al. 2005, Wu et al. 2002), human respiratory epithelial cells (Shah et al. 2009) and human airway smooth

muscle cells (An et al. 2012, Deshpande et al. 2010). T2Rs present in gut interact with bitter ligands and cause stimulation of hormone secretion from enteroendocrine cells (Dotson et al. 2008, Jeon et al. 2008, Le Neve et al. 2010). T2Rs increase ghrelin release after an oral gavage (Janssen et al. 2011) which suggest that T2Rs play a crucial role in controlling satiety, metabolism, gastric emptying and food intake. In a study by Deshpande et al. 2010, it was shown that T2R agonists caused bronchodilation of the airways which was three times more than the effect caused by beta-adrenergic agonists. Relaxation of the airway smooth muscles in lungs was exhibited even in case of $beta_2$-adrenergic receptor tachyphylaxsis, when T2R was activated (An et al. 2012). This effect of T2Rs was proposed as a novel therapeutic approach in overcoming chronic obstructive lung disease and bronchospasm in asthma (An et al. 2012). Another study (Shah et al. 2009) showed that T2Rs play a crucial role in enhancing the beating of motile cilia, which in turn might be crucial for the clearance of cellular debris or toxins from airways.

1.2 Tastants / Ligands

A large number of compounds are sensed as bitter by humans (Meyerhof et al. 2010). However, there are only 25 T2Rs which recognize a wide range of bitter compounds, implying that each T2R is tuned to respond to an array of bitter stimuli. A vast array of structurally diverse compounds are recognized by T2Rs including- azacycloalkanes, fatty acids, hydroxy fatty acids, amino acids, alkaloids, steroids, peptides, metal ions, N-heterocyclic compounds, carbamides, amines, terpenoids, esters, carbonyl compounds, halogenated or acetylated sugars, crown ethers, secoiridoids, glycosides, thioureas, ureas, lactones, flavanoids and phenols (Belitz H-D 1985, DuBois GE 2008). Recently, it was suggested that T2Rs differ substantially in their tuning breadth, ranging from broadly tuned to extreme selectivity (Meyerhof et al. 2010). Approximately, half of the fifty eight natural

bitter compounds tested were recognized as bitter by T2R10, T2R14 and T2R46 implying their broad substrate range. This molecular detection range and the presence of abundant allelic forms of T2Rs may account for the perception of various ligands as bitter (Behrens and Meyerhof 2009, Behrens et al. 2004, Brockhoff et al. 2007, Kuhn et al. 2010, Meyerhof et al. 2010). On the other hand, T2R4 is very specific and senses a limited number of bitter ligands (Chandrashekar et al. 2000). Recently, aromatic quinolines, amine derivatives and salts, purine analogs and sesquiterpene lactones were shown to activate T2R4. However, only threshold values and not the EC_{50} values for most of the agonists that activate T2R4 were reported (Meyerhof et al. 2010). These include drugs like quinine, colchicine, diphenidol and azathiopurine. Quinine, a natural alkaloid was identified to be one of the most potent bitter tasting molecules (Singh et al. 2011b). Quinine was shown to activate T2R4 with highest efficacy (Pydi S. P. et al. 2012). Quinine was found to activate nine T2Rs including T2R4, T2R7, T2R10, T2R14, T2R31, T2R39, T2R40, T2R43 and T2R46 (Meyerhof et al. 2010).

1.3 T2R signaling pathway

The interaction of an agonist or ligand with the transmembrane domain of T2R initiates taste signal transduction. McLaughlin et al., reported that the α-subunit of the heterotrimeric G-protein, i.e. α-gustducin, is the cognate taste specific G-protein (McLaughlin et al. 1992). The taste specific heterotrimeric G-protein is made up of α-gustducin, β3, γ13 subunits (Adler et al. 2000, Wong et al. 1996). In the inactive state, the α-gustducin is bound to GDP. Binding of agonist causes a conformational change in T2R, leading to exchange of GDP to GTP on the α-gustducin and also to the dissociation of βγ dimer from the G-protein. The α-gustducin was suggested to stimulate phosphodiesterase (PDE) leading to decrease in cAMP levels (Margolskee 2002, Yan et al. 2001).

On the other hand the G-βγ complex activates PLCβ2 and leads to the production of diacylglycerol (DAG) and inositol triphosphate (IP_3) (Clapp et al. 2001). IP_3 in turn stimulates IP_3 receptors present on the endoplasmic reticulum causing release of intracellular calcium. Increased Ca^{2+} levels activate TRPM5 channels and results in fluctuation of membrane currents causing influx of sodium ions (Ishimaru and Matsunami 2009). This leads to generation of action potential (depolarization of cell) and release of neurotransmitter (Margolskee 2002, Roper 2007). High performance liquid chromatography (HPLC) showed that serotonin is the neurotransmitter involved in taste transduction (Zancanaro et al. 1995). The final events in this pathway are yet to be determined and the complete pathway still needs to be properly elucidated.

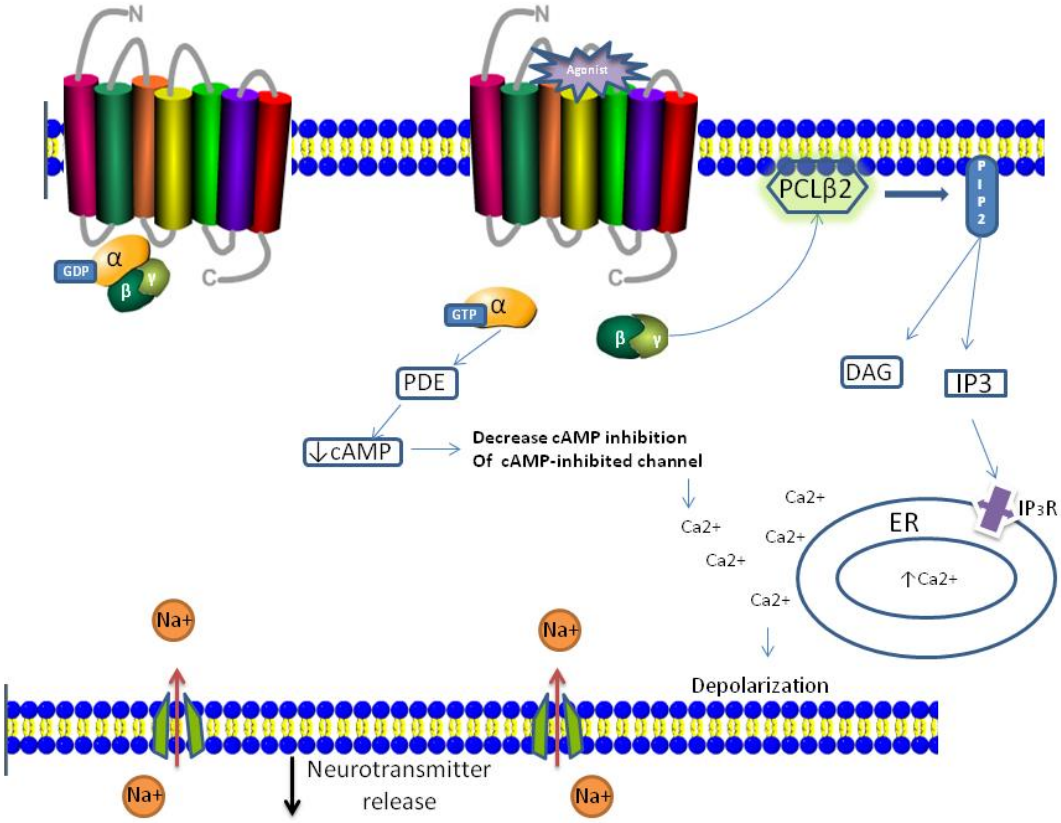

Figure 6. Bitter taste signal transduction mechanism
Bitter agonists stimulate T2Rs, which in turn activate gustducin. The GDP bound to α-gustducin triggers PDE resulting in decreased cAMP levels. Following this the intracellular levels of calcium are elevated leading to depolarization. On the other hand, Gβγ heterodimer activates PLCβ2 to produce IP_3. This triggers the IP_3 receptor on the ER and results in raised intracellular calcium levels.

CHAPTER TWO

RATIONALE AND OBJECTIVES

2.1 Rationale

T2Rs are known to recognize large number of structurally diverse bitter compounds. This interaction with diverse chemical ligands requires the binding pockets of T2Rs to be flexible as well as selective. Structure-function studies of T2Rs are essential in elucidating their affinity for various bitter compounds and in demonstrating the activation mechanism of T2Rs. Use of chimeric receptors, molecular modelling studies, and site directed mutations of these receptors followed by calcium assays (functional assay) helped in determining receptor regions and amino acid residues responsible for activation of T2Rs such as T2R1 (Singh et al. 2011b, Upadhyaya et al. 2010), T2R10 (Born et al. 2013), T2R16 (Sakurai et al. 2010b), T2R30 (Pronin et al. 2004), T2R31, T2R38, T2R43, T3R44 and T2R46 (Brockhoff et al. 2010).

The focus of this study is the T2R4 receptor. The rationale for choosing this receptor is as follows:

Compared to other T2Rs, T2R4 is selective in nature and binds to a limited number of ligands (Chandrashekar et al. 2000). Thus far, approximately 16 ligands are known to activate T2R4.

It was shown by RT-PCR analysis and immuno-histochemistry that T2R4 is localized in extra-oral tissues including the brain (Singh et al. 2011a). The role of T2R4 in the extra-oral tissues remains to be elucidated.

Structure-function studies on T2R4 are very limited (Pydi S. P. et al. 2012, Pydi S. P. et al. 2013) and information on ligand binding pocket of T2R4 is lacking. To elucidate this, quinine was chosen as it was found to be the most bitter compound. Information on binding sites will help to elucidate, how so few T2Rs, are able to recognize numerous bitter tastants.

2.2 Specific objectives of this project

2.2.1 Specific objective 1:

To build a three dimensional model of T2R4, and elucidate its potential ligand binding pocket.

2.2.2 Specific objective 2:

To characterize agonist (quinine) binding in T2R4 by a combination of techniques including, site-directed mutagenesis, analysis of receptor expression and functional assays on the mutants using calcium imaging.

CHAPTER THREE

MATERIALS AND METHODS

3.1 Materials

Mammalian tissue culture medium products such as Dulbecco's Modified Eagle Medium /F12 (DMEM/F12) high glucose media and OptiMEM were purchased from Gibco/Life technologies (Carlsbad, CA, USA), fetal bovine serum (FBS) was from Sigma (St. Louis, MO, USA). Penicillin/Streptomycin/Glutamine (PSQ) was from Invitrogen. Nano drop 2000 instrument was purchased from Thermo Scientific. Cell culture dishes were purchased from Corning Life Sciences (Lowell, MA,USA). 1.5 ml, 50 ml disposable plastic conical tubes (Falcon tubes) and 96 well black walled with clear bottom microtiter plates were from International BD Biosciences (Mississuaga, ON, Canada). RedGel Nucleic Acid stain, 10,000X in water was purchased from Biotinum. Nucleic acid purification kits were from QIAGEN (Toronto, ON).

Gα16-gustducin44 (Gα16/44) chimera was a kind gift from Dr.Takashi Ueda, Nagoya City University, Japan. Lipofectamine 2000 and pcDNA 3.1 were from Life technologies. Restriction enzymes were from New England Biolabs (Ipswich, MA, USA). Automated cell counter and Electrophoresis instrument were from Bio-Rad Laboratories (Mississauga, ON). TAS2R4 and its mutant genes were generated using commercial service from GenScript Inc., (MA, USA).

Calcium sensitive dye Fluo-NW (no wash) was from Life technologies (Carlsbad, CA, USA). Quinine hydrochloride was purchased from Sigma. Consumables for the Flexstation-3 fluorescence microplate reader, such as the dispensing black tips were purchased from Molecular devices (Sunnyvale, CA, USA).

3.2 Composition of buffers and media

Buffers

Agarose loading buffer: 3.3 ml 150 mM Tris, pH 7.6, 25 mg bromophenol blue, 6 ml glycerol, 0.7 ml H_2O to make up to 10 ml.

Phosphate Buffered Saline (PBS) 10X: 2.4 g $Na_2HPO_4.7H_2O$, 80 g NaCl, 2.4 g KH_2PO_4 and 2 g KCl dissolved in 800 ml H_2O, pH was set at 7.4 and volume was made up to 1 litre.

Phosphate Buffered Saline (PBS) 1X: 100 ml of 10X stock was diluted with 900 ml H_2O.

TAE (Tris Acetate-EDTA): 1.1 ml glacial acetic acid, 4.84 g Tris, 2 ml 0.5 M Na_2EDTA (pH 8.0) and water to make to 1 litre.

1% Bovine Serum Albumin (BSA) in 1x PBS.

2% BSA in 1x PBS.

Media

DMEM/F12: DMEM High Glucose/ F-12 (1:1), Gibco, Life technology.

DMEM/F12 + : DMEM High Glucose/ F-12 (1:1, Gibco, Life technology) supplemented with 10% heat inactivated (37°C for 4 hour) FBS.

DMEM/F12 + + : DMEM High Glucose/ F-12 (1:1, Gibco, Life technology) supplemented with 10% heat inactivated (37°C for 4 hour) FBS and 1% PSQ.

Luria-Bertani (LB) media: 5 g/l Yeast extract and 10 g/l Tryptone.

3.3 Methods

3.3.1 Preparation of LB–ampicillin plates

To prepare petri dishes for *Escherichia Coli* (*E.coli)* growth, 20 g LB-agar powder was dissolved in 500 ml of distilled water in a 1L flask and autoclaved for 40 min.

Autoclaved medium was cooled down on a stirrer/hot plate (Corning PC-420D) with constant stirring at room temperature for 30 minutes and 500 µl of 100 mg/ml ampicillin solution was added. 20 ml of this mixture was poured into each sterile petri plates and allowed to solidify for approximately 5 hrs at RT. These plates were stored at 4°C until further usage.

3.3.2 Wild type TAS2R4 and mutants

The synthetic TAS2R4 gene codon optimized for expression in mammalian cells was synthesised commercially (GenScript, MA, USA). The gene has an N-terminal FLAG tag for detection by the FLAG antibody. The gene sequence along with the protein sequence is shown in figure 8. The gene is flanked by EcoRI and NotI restriction sites at the 5' and 3' ends. It is cloned into the EcoRI-NotI site of the multiple cloning site region of the mammalian expression vector pcDNA 3.1 (Figure 7). The mutants were introduced into this gene using a commercial service (GenScript Inc., MA, USA).

3.3.3 Transformation of competent *E. coli*

A vial of *E.coli* competent cells (stored at -80°C) was thawed on ice. 50 µl of these cells was transferred to 1.5 ml eppendorf tube and 2 µl of DNA (wild type or mutant) was added to the eppendorf tube, and kept on ice for 30 min. These cells were given heat shock by incubating the tubes at 42°C for 45 sec on a multi-temperature water bath and immediately cooled on ice for about 2 min. This step is done to make the membranes of *E.coli* porous and permeable to the DNA. 450 µl of LB broth was added to each tube and the tubes placed at 37ºC for 1 hr with vigorous shaking set at 175 rpm. 100 µl of the mixture from each tube was spread on pre-warmed LB-agar plates and kept aside for 5-10 min. Later, these plates were kept at 37°C for overnight. The following day individual bacterial

colonies were picked and inoculated in 5 ml of LB media containing 5 µl of 100 mg/ml ampicillin solution, and allowed to grow overnight at 37°C with vigorous shaking at 175 rpm in an orbital shaker.

3.3.4 Plasmid DNA extraction from *E.coli*

Plasmid DNA was purified from *E.coli* cultures in either small amounts by using QIAprep Spin miniprep Kit or in large quantities by QIAGEN plasmid Maxi Kit.

3.3.4.1 Isolation of plasmid DNA using QIAprep spin

From 5 ml of the overnight grown cultures, 1.5 ml culture was taken in a 1.5 ml plastic tube and pelleted by centrifugation. Pelleted bacterial cells were resuspended in 250 µl of buffer P1 and vortexed. 250 µl of buffer P2 was added and mixed by inverting the tube 4-6 times until a clear solution is obtained. To allow the lysis reaction to proceed, the tube was kept aside for 5 min. The solution in the tube turns blue (due to the presence of LyseBlue reagent in buffer P1) indicating that bacterial cell lysis has occurred. 350 µl of buffer N3 was added and mixed instantly and thoroughly by inverting the tube 4-6 times. The solution then turns colorless indicating neutralization of the reaction condition in the tube. This mixture was centrifuged in a table top microcentrifuge for 10 min at 13,000 rpm. The supernatant from above step was decanted into QIAprep spin column and centrifuged for 30-60 sec and the flow-through was discarded. This spin column was washed by adding 500 µl buffer PB and centrifuged for 30-60 sec and the flow-through was discarded again. 750 µl buffer PE was added to the spin column and centrifuged for 30-60 sec and the flow-through was discarded. To get rid of residual wash buffer, the spin column was centrifuged for 1 min. This spin column was placed in a clean 1.5 ml tube and 25 µl of autoclaved water was added to the centre of the spin column and kept aside for 1 min. The plasmid DNA was eluted by centrifuging the spin column in the 1.5 ml tube.

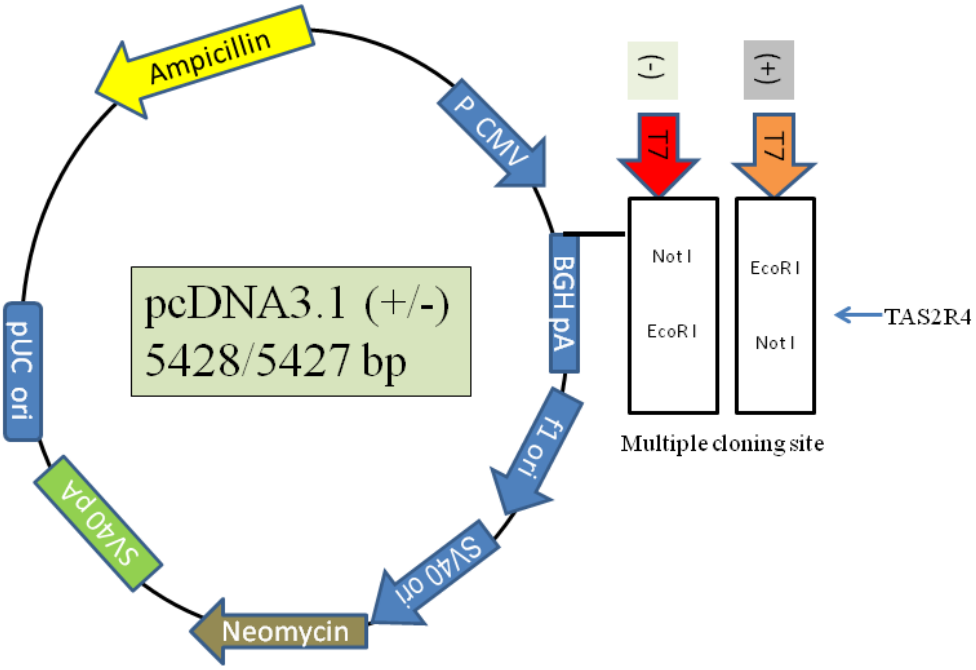

Figure 7. Vector map of pcDNA 3.1 inserted with TAS2R4 gene
The expression vector pcDNA 3.1 of 5.4 kb, containing the commonly used human cytomegalovirus immediate-early (CMV) promoter for high-level expression in mammalian cells is shown. TAS2R4 gene (924 bp) is cloned into the EcoRI-NotI site of the multiple cloning site region of the mammalian expression vector pcDNA 3.1. TAS2R4 gene is flanked by EcoRI and NotI restriction sites at the 5' and 3' ends. DNA of WT-TAS2R4 and its mutants were introduced into this gene using a commercial service.

3.3.4.2 Isolation of plasmid DNA using QIAGEN Maxiprep

High purity DNA in large amounts is needed for mammalian cell transfections. To obtain this, 1 ml overnight *E.coli* cultures harboring the respective plasmid DNA i.e., wild type or mutant gene in plasmid pcDNA 3.1 was inoculated in 100 ml of fresh LB media containing 100 µl of ampicillin in a conical flask. This was grown at 37ºC with vigorous shaking for 18 hrs until it reache A_{600} of 0.6. The conical flask was kept on ice and the culture was transferred to 50 ml disposable plastic tubes. To harvest the cells in bulk, the 50 ml tubes were centrifugated using SLA 1500 rotor in Sorvall RC 6 centrifuge and rotated at a speed of 6,000 x g for 15 min at 4°C. The plasmid DNA was extracted from bacterial pellet using QIAGEN Plasmid Maxi Kit.

10 ml of Buffer P1 was used to resuspend the bacterial cell pellet by vigorous vortexing. 10 ml of Buffer P2 was added to this and mixed thoroughly by inverting the tube 4-6 times. The tube was set aside for 5 min at room temperature. 10 ml of Buffer P3 (pre-chilled to 4°C) was added to the tube and mixed by inverting 4-6 times vigorously. This was incubated on ice for 20 min. To clear the bacterial lysate, the above solution was centrifuged at 20,000 x g for 35 min at 4°C. Meanwhile, the QIAGEN-tip was equilibrated by applying 10 ml of Buffer QBT. The QIAGEN-tip was allowed to empty by gravity flow. The supernatant of the cleared lysate solution was applied to the QIAGEN-tip and it was allowed to enter the resin by gravity flow. The QIAGEN-tip was washed with 2 x 30 ml of Buffer QC, where the buffer was allowed to move by gravity flow.

DNA was eluted from the QIAGEN-tip by adding 15 ml of buffer QF. To precipitate the eluted DNA, 10.5 ml of room temperature isopropanol was added to the tube and mixed. The tube was centrifuged at 17,000 x g for 35 min at 4°C. The supernatant was decanted carefully. The DNA pellet obtained was washed with 5 ml of 70% ethanol and centrifuged

at 17,000 x g for 10 min at 4°C. The supernatant was decanted and the pellet was air dried for 5-10 min, and the DNA was redissolved in suitable volume of autoclaved water.

To confirm the correct insert, the DNA obtained was subjected to restriction enzyme digestion using mixture of 2-3 µl of DNA, 1 µl BSA (10X), 1 µl of EcoRI buffer (NEB), 1 µl NotI, 1 µl EcoRI (20,000 U/ml) and made upto a final volume of 10 µl with water. This mixture was incubated at 37°C for 2-3 hrs. This was followed by analysis using agarose gel electrophoresis.

3.3.5 Agarose gel electrophoresis

A 1% agarose gel was prepared by dissolving 500 mg of agarose in 50 ml TAE by heating for 45 sec in a microwave, shaken and reheated for 45 sec. To this 1 µl of GelRed Nucleic Acid Gel stain was added and mixed. This solution was poured in the Bio-Rad Sub Cell horizontal electrophoresis tray. A comb was inserted immediately and this was allowed to solidify for about 1 hr. 1 µl of loading buffer was added to 10 µl of DNA sample and this was loaded on the gel. For molecular weight size standards, 1 kb plus DNA ladder (New England Biolabs) was used. The apparatus was set at 111 V and this was allowed to run until bromophenol dye had migrated to two-thirds of the gel length. The bands obtained were visualized with UV light using Bio-Rad Gel Doc. The DNA samples showing appropriate banding pattern were selected for further analysis.

3.3.6 Preparation of glycerol stocks

To 1 ml of the *E.coli* overnight cultures with the correct transformants or plasmids 1 ml of 50% glycerol (tissue culture grade) was added and the vials were stored at -70°C until further use. Culturing of *E.coli* from the glycerol stocks is as follows. Small amount of stock was picked with an autoclaved stick and inoculated in test tube containing 5 ml of LB media

with 5 µl of ampicillin (100 mg/ml) and vigorously shaken at room temperature for 16-18 hrs in a shaker. This was subjected to miniprep or maxiprep to isolate the plasmid DNA. The concentration and purity of DNA (A_{260}/A_{280} ratio) was checked using nanodrop (Thermo Scientific).

3.3.7 Expression of TAS2R4 in Human Embryonic Kidney (HEK293T) cells

Human embryonic kidney cells (HEK293T) were utilized as they are immortalized cells and stably express the large T-antigen of SV40. Plasmids such as pcDNA 3.1 contain the SV40 origin and are replicated to a high copy number of more than 400 per cell. This makes HEK293T cells suitable for heterologous expression of many mammalian proteins. The cells were grown at 37°C with 5% CO_2 in 10 cm round dishes in 10 ml DMEM++ medium till they were 70- 80% confluent. These cells were split and plated in 6 well plates (2 ml DMEM++/well) for co-transfection. Constructs of TAS2R genes in pcDNA 3.1 together with Gα 16/44 were used for transfection. Only pcDNA3.1 without TAS2R4 gene was used as mock. Initially, 3ug of each DNA : Gα 16/44 (1:1 ratio) was dissolved in 200 µl of OptiMEM in individual tubes. In a different tube, lipofectamine 2000 at 2:1 ratio lipofectamine vs DNA was dissolved in 200 µl OptiMEM (per sample). After 5 min of incubation at room temperature, lipofectamine 2000 was added to the DNA and set aside for 20 min at room temperature. DMEM/F12 medium was added to each sample to make the volume 2 ml. This mixture was added to 6 well plates containing HEK293T cells and incubated for 6-8 hrs at 37°C with 5% CO_2.

3.3.8 Calcium assay

For functional characterization of T2R4 and mutants, intracellular calcium mobilized was measured using Flexstation-3 fluorescence plate reader (Molecular Devices, CA, USA).

HEK293T cells were transiently transfected with 3 µg of DNA (WT-TAS2R4 or pcDNA or mutants) and 3 µg of Gα 16/44 using lipofectamine 2000. After 6-8 hrs of transfection, the samples were centrifuged at 350 x g, 4 min at 4°C. Approximately, 1.5 x 10^5 cells/well were plated in a 96-well tissue culture treated BD-falcon biolux microplate. Following 14-16 hrs of incubation at 37°C, the medium was replaced with 100 µl of 1 x concentration of Fluo-4NW dye, consisting of 10.5 ml assay buffer and 100 µl of 2.5 mM concentration of probenecid. Fluo-4NW dye requires no washing steps and gives calcium measurement in high throughput screening applications. To reduce the loss of dye from the cell, probenecid was used as it inhibits the transport of organic anion. The plate was kept at 37°C for 45 min followed by 45 min at room temperature. An assay compound plate consisting of 96 wells was used to occupy different concentrations of quinine. Buffer alone was used for measuring basal activity of T2R4. Flexstation-3 fluorescence plate reader set at 525 nm proceeding excitation at 494 nm was used to measure the fluctuations in intracellular levels of calcium to determine T2R4 activity. Calcium mobilized was expressed in relative fluorescence units (RFU) followed by subtraction of responses obtained from control cells (contain pcDNA 3.1 and Gα 16/44 construct). Dose-response curves were constructed and calculation of EC_{50} was determined by nonlinear regression using PRISM software version 4.03 (GraphPad Software Inc, San Diego, CA, USA).

3.3.9 Flow cytometry

Cell surface receptor expression was analyzed by Flow cytometry using BD FACS Canto flow cytometer. HEK293T cells were transiently transfected with 6 µg of DNA per $5x10^6$ cells with either TAS2R4 or mutants using lipofectamine 2000 as described previously with DNA to Lipofectamine ratio (1:2). Briefly, 22-24 hrs post transfection, approximately $1x10^6$ of live cells were counted in Bio-Rad cell counter machine using

trypan blue as dye and taken into 15 ml tube and placed on ice. The cells were then incubated with mouse monoclonal anti-FLAG, M2 primary antibody (1:500 dilution) in PBS for 1 hr on ice. The cells were then washed by centrifugation at a speed of 250 x g for 3 min at 4ºC, and the washing step was repeated for 2 to 3 times. The cells were then incubated with (1:1000 dilution) of secondary antibody Alexa 488 goat anti-mouse for 1 hr in dark, on ice. Cells were washed 3 to 4 times using centrifugation at 250 x g for 3 min at 4ºC with PBS (1X) and were re-suspended in 200 µl of PBS (1X). The fluorescence signal of $1x10^4$ cells/tube were measured using single colored analysis by BD FACS Canto flow cytometer. The cell surface receptor expression was calculated as a percentage of WT-TAS2R4 expression set at 100% after deducting the values obtained from mock transfected cells. The user settings used were forward scatter (FSC) 137 Volts, side scatter (SSC) 303 Volts, and voltage of Alexa488 was set to 294 V. The results were analyzed using FACS Diva software and represented in mean fluorescence intensity ± SEM (MFI ± SEM).

3.3.10 Molecular modeling

Protein molecular modeling utilizes both theoretical and computational methods to explore the topology, dynamics, structural orientation and thermodynamics of proteins. In this study, modeling was used to elucidate the ligand binding pocket and conformational changes undergone by T2R4. As the three dimensional structure of T2R4 is unknown, homology modeling was performed. In this homology modeling, amino acid sequence alignment and crystal structure of rhodopsin were used to build the model of T2R4. Rhodopsin PDBID: IU19 obtained from protein bank was utilized as a template to construct a three dimensional model of T2R4. Among the GPCR crystal structures available, both rhodopsin and T2R4 share more homology compared to others. Evidence suggests that in homologues, the structure of proteins was more conserved than the sequence of its amino

acids (Chothia and Lesk 1986). The loop regions in T2R4 which were not aligned in sequence with rhodopsin were loop modeled. T2R4 model was built in inactive state where amino acid sequences without the FLAG tag were utilized. Pymol was used to introduce structural waters into this model. SYBYL-1.3 molecular modeling suite (Tripos Inc, USA) was used to conduct molecular dynamics simulations (10 ns) on the receptor models. PROCHEK was used to analyse the quality of model and 98% of the residues were shown to be in the favorable regions of the Ramachandran plot.

3.3.11 Autodock Vina

Once the 3D structure of T2R4 was generated, its interaction with quinine was studied using a technique called molecular docking. AutoDock Vina software was used to determine the accurate binding modes of quinine docked to T2R4 receptor. The extracellular surface of the protein was chosen for placing the grid box of dimensions 25 x 25 x 28 (Angstrom) with centre grid boxes aligning 52.67, 68.9, 48.77 in X, Y and Z dimensions respectively. 40 genetic algorithms were run for the quinine and in each run the best orientation was saved. Ultimately, all the poses were superimposed and the most frequent orientation of quinine was selected as final pose. The T2R4 - Quinine complex was energy minimized by 2000 steps of conjugate gradients. This 3D structure of T2R4-Quinine complex was used in further studies. The amino acids of T2R4 showing interaction with quinine and those falling within 4Å region were mutated. This was done to elucidate the importance of the interacting residues in T2R4 involved in quinine binding.

3.3.12 T2R4 mutants

Based on the molecular models, the following 12 T2R4 mutants- A90G, A90F, F91A, F92A, Y155A, N173A, N173Q, T174A, T174S, Y258A, K270A, K270R, were

synthesized and functionally characterized. The amino acid sequences of mutants were generated using DNA sequence to protein sequence translating program (http://www.fr33.net/translator.php), where the sequence of wild type T2R4 with FLAG tag was used as the source (Figure 8).

Figure 8. Nucleic acid (DNA) and amino acid sequence of T2R4
Shown is the DNA and the corresponding amino acid sequence of the FLAG-T2R4 and mutants. The TAS2R4 gene is flanked by EcoRI and NotI restriction sites (blue), a kozak sequence (yellow) before, and a FLAG sequence immediately after, the start codon (ATG). The position of the mutants and the codon change are shown. The TAS2R4 gene and the mutants are synthesized commercially.

CHAPTER FOUR

RESULTS

4.1 DNA manipulation

The plasmid DNA of the WT-TAS2R4 and mutants in vector pcDNA 3.1 was digested with restriction enzymes EcoRI and NotI, and the products analyzed by agarose gel electrophoresis, as described in Methods. The size of the WT-TAS2R4 or mutant gene is 924 base pairs. When this gene was inserted into the vector pcDNA 3.1 (5.4 kb), the size of the plasmid DNA (vector + gene) is around 6.3 kb, as observed on a 1% agarose gel. The empty vector pcDNA 3.1 cut with EcoRI and NotI was used as control, where the absence of a band at around 1 kb can be observed (Figure 9). The DNA of the plasmids of different mutants analyzed in this study, and after digestion with EcoRI and NotI showed a band at around 1 kb, which is of the expected size (Figure 9). Nine mutants, A90G, A90F, F91A, F92A, Y155A, N173A, T174A, T174S and K270A are shown in Figure 9. Other mutants N173Q, Y258A and K270R were also in the 1 kb range (data not shown).

4.2 Secondary structure and homology model of T2R4

The secondary structure of T2R4 amino acid sequence is shown in Figure 10. The native receptor consists of 299 amino acids. The receptor is made up of a short N-terminus on the extracellular side, 7 transmembrane (TM) helices, 3 extracellular loops (ECLs) and 3 intracellular loops (ICLs), and a C-terminus on the intracellular side. TMpred software tool was used to predict the TM regions. There are 307 amino acids in the coding region of T2R4 including the FLAG octapeptide tag at the N-terminus. In addition to the seven TM helices, TMpred predicted two short helices on the cytoplasmic side, one in the ICL2, and the other in the C-terminus which runs parallel to the membrane surface, in T2R4. A homology model

of T2R4 was built using a rhodopsin template, and the agonist quinine was docked to it, as described in methods (Figures 10 and 11).

4.3 Mutagenesis guided by molecular model of T2R4

To elucidate the amino acids involved in quinine binding in T2R4, a molecular model guided mutagenesis approach was followed. A number of amino acid residues present on the extracellular side of T2R4 were predicted to be involved in binding to quinine. These include residues from TM3, TM4, TM6 and ECL3 interface, TM7 and ECL3 interface, and ECL2. Quinine was found to have hydrogen bond interactions with Asparagine 173 (N173), Threonine 174 (T174) and backbone amine-group of Alanine 90 (A90). In addition, amino acids found in the 4Å region surrounding the binding pocket also influence the interaction between quinine and T2R4; they were also taken into consideration. They include Phenylalanine 91 (F91), Phenylalanine 92 (F92), Tyrosine 155 (Y155), Tyrosine 258 (Y258) and Lysine 270 (K270) (Figures 10 and 11). Two types of mutations were made in T2R4. First, mutations were made to a smaller amino acid such as alanine or glycine (if the amino acid being mutated is an alanine); with the expectation that this substitution will have minimal effect on receptor folding and ligand binding. Second, mutations were made with either a non-conserved substitution such as alanine to phenylalanine or with conserved substitution such as lysine to arginine. The following mutants were generated A90G, A90F, F91A, and F92A on TM3, Y155A on TM4, N173A, N173Q, T174A, and T174S on ECL2, Y258A at TM6 and ECL3 junction, K270A and K270R at TM7 and ECL3 junction. These mutants were characterized for their expression and function.

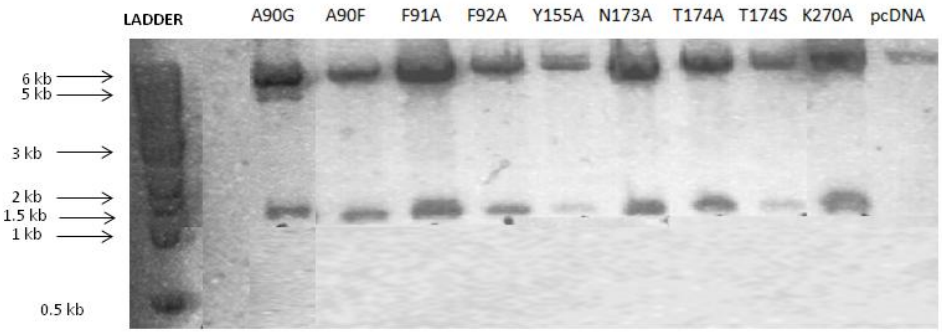

Figure 9. Agarose gel electrophoresis of WT-TAS2R4 and its mutants. pcDNA 3.1 containing TAS2R4 gene or mutants was digested with EcoRI and NotI restriction enzymes and the products analyzed on a 1% agarose gel. A 1 kb plus DNA ladder (New England Biolabs) is shown in the first lane, and empty vector pcDNA 3.1 used as a control, is shown in the last lane. All the constructs showed two bands, one at around 5 kb which corresponds to the vector, and a second band at ~1 kb which is the gene (WT-TAS2R4 or mutant of interest). The control (last lane) cut with EcoRI and NotI showed no insert in the 1 kb region.

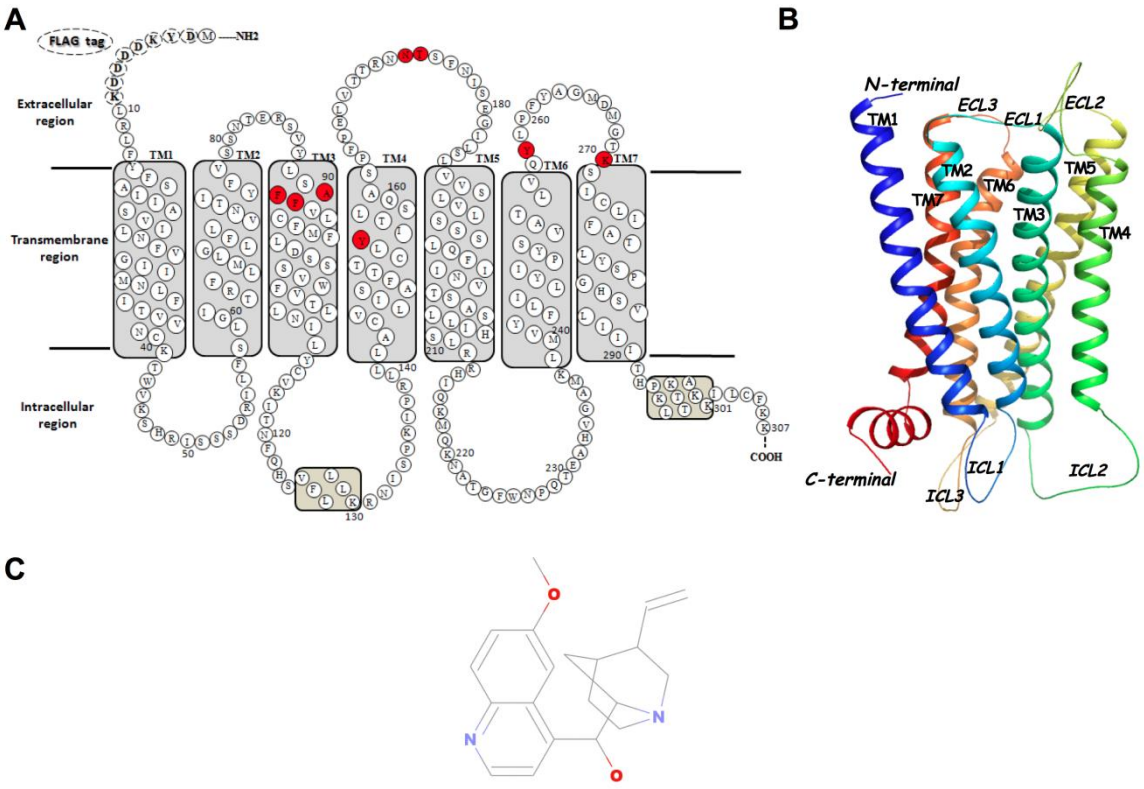

Figure 10. Models of the T2R4 and quinine. A. Secondary structure model of T2R4 amino acid sequence. T2R4 receptor used in this study consists of 307 amino acids including the FLAG-octapeptide sequence located at the N-terminus. Residues important in agonist (quinine) binding were represented in red color. **B.** Three-dimensional model of T2R4. The seven transmembrane helices are shown in different colors. T2R4 three-dimensional model was built using rhodopsin crystal structure as template. **C**. Chemical structure of quinine. Quinine is a natural alkaloid with bitter taste. Three dimensional chemical structure of quinine which is known to act as a potential agonist was used for docking to T2R4 receptor. Quinine consists of aromatic quinoline and bicyclic quinuclidine rings fused together.

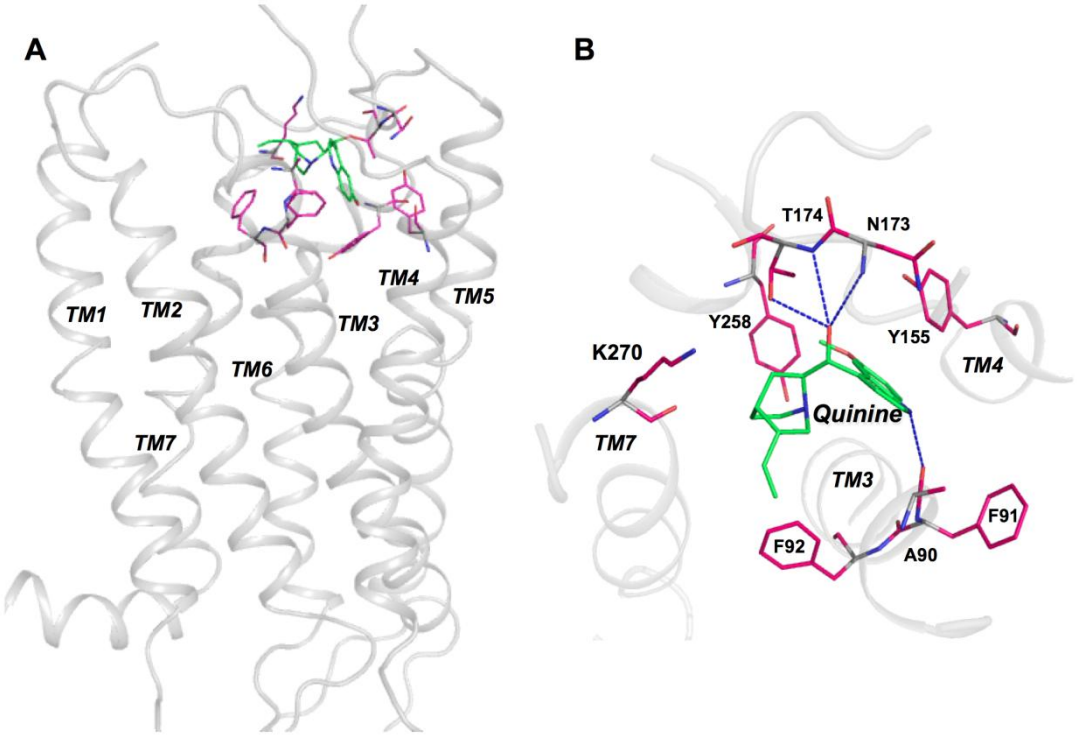

Figure 11. Molecular model of T2R4 bound to quinine. A. Model of T2R4-quinine complex. T2R4 and quinine are shown in grey and green colors respectively. The residues involved in ligand binding are shown in pink color. **B.** Amino acids within 4 Å region of quinine in T2R4. T2R4 molecular model was docked with quinine (green) and the interacting residues (pink) were represented as sticks using PyMol. A90, N173 and T174 formed hydrogen bonds with quinine. Blue dotted lines represent the H-bonds and the TM regions are represented in gray color.

4.4 Characterization of the expression of the WT-T2R4 and its mutants

Proper cell surface expression of a GPCR is normally used as an indicator of correct protein folding. The T2R4 construct used in this study had a FLAG-tag at its N-terminus which allowed detection of the receptor on the cell surface by an anti-FLAG antibody, without the need to permeabilize the cells. Using flow cytometry, the cell surface expression of WT-T2R4 and its mutants was analyzed. The values were shown in mean fluorescence intensity (MFI) ± SEM after deducting MFI from mock transfected cells (Table 2). The MFI values obtained were normalized to the WT-T2R4, and expressed in percentage (Figure 12). Majority of the mutants A90G, F91A, N173Q, T174S, Y258A and K270R showed proper expression on the surface of HEK293T cells. The expression levels of these mutants were similar to WT-T2R4. The mutants Y155A, N173A and T174A showed 30%-40% increased expression levels compared to that of WT-T2R4. While three mutants A90F, F92A and K270A, showed upto 40% decrease in cell surface expression. However, no statistical significance in expression levels between the different mutants and WT-T2R4 was observed (Figure 12).

4.5 Functional characterization of the WT-T2R4 and ligand binding pocket mutants

The natural alkaloid quinine is one of the most intense bitter tasting compounds, and is an agonist for T2R4. As shown in Figure 13, quinine stimulated T2R4 and caused a concentration-dependent increase in intracellular calcium in cells with an EC_{50} value of 627 ±80 µM. Functional analysis of WT-T2R4 and mutant receptors were determined by measuring changes in intracellular calcium of HEK293T cells transiently expressing these receptors, after application of different concentrations of quinine. The mutants displayed varied levels of signaling (Figures 14 to 25).

Table 2: Mean fluorescence intensity (MFI) of T2R4 and its mutants as determined by flow cytometry.

SAMPLE	MFI value
T2R4	**100**
A90G	**95±15**
A90F	**67±5**
F91A	**85±17**
F92A	**59±12**
Y155A	**140±9**
N173A	**129±5**
N173Q	**105±14**
T174A	**126±9**
T174S	**91±12**
Y258A	**107**
K270A	**71±3**
K270R	**105±2**

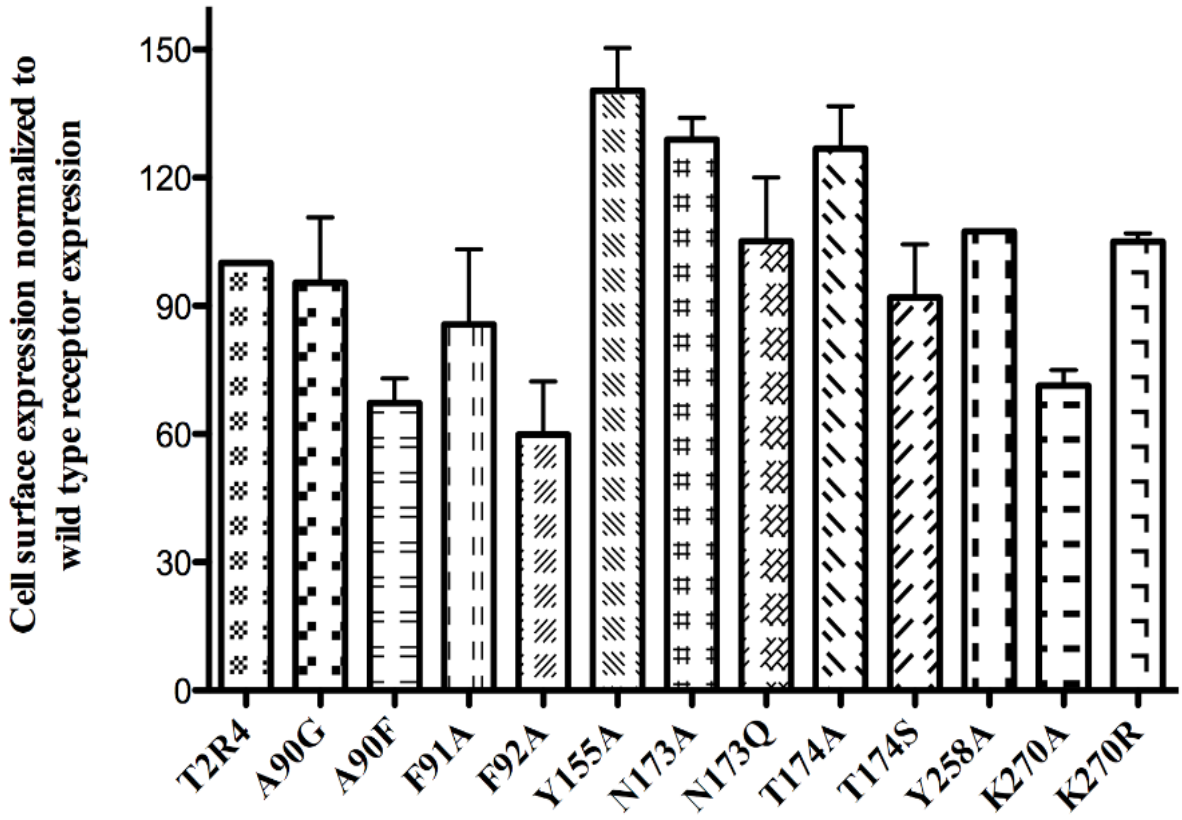

Figure 12. Cell surface expression of WT-T2R4 and its mutants. Cell surface expression is shown on Y-axis versus samples on X-axis. The MFI values were subtracted from mock transfected (pcDNA 3.1) HEK293T cells and normalized to WT-T2R4 considered as 100%.

Mutation of Alanine 90 showed interesting results (Figures 14 and 15). The A90G mutant, where alanine was replaced with a simple amino acid glycine which has no functional group, quinine treatment resulted in no detectable calcium mobilization compared to WT-T2R4 (Figure 14). However, replacement of the alanine with a bulky aromatic phenylalanine, as in A90F mutant, resulted in a hyperactive mutant with an upward shift of the dose-response curve, as seen in Figure 15. The F91A mutant did not display a quinine dependent increase in calcium mobilization, while the F92A showed a response similar to WT-T2R4, with an EC_{50} value of 810 ±150 µM (Figures 16 and 17).

Analysis of the TM4 and ECL2 mutations Y155A, N173A, N173Q, T174A and T174S, showed that except for T174S, none of the other mutants displayed a quinine dependent increase in calcium mobilization (Figures 18-22). The T174S mutant showed a right shift in the dose-response curve and close to a two-fold increase in EC_{50} value of 1612 ±395 µM compared to 627 ±80 µM for WT-T2R4 (Figure 22). The two residues present on ECL3 and are predicted to play a role in quinine binding are Y258 and K270. The Y258A mutant displayed no quinine dependent calcium mobilization (Figure 23). Interestingly, the K270A mutant was hyperactive, and showed an upward and rightward shift in the dose-response with more than a two-fold increase in EC_{50} value of 1497 ±310 µM (Figure 24). The complementary mutation, K270R, showed similar dose response as WT-T2R4 with an EC_{50} value of 780 ±180 µM (Figure 25).

A.

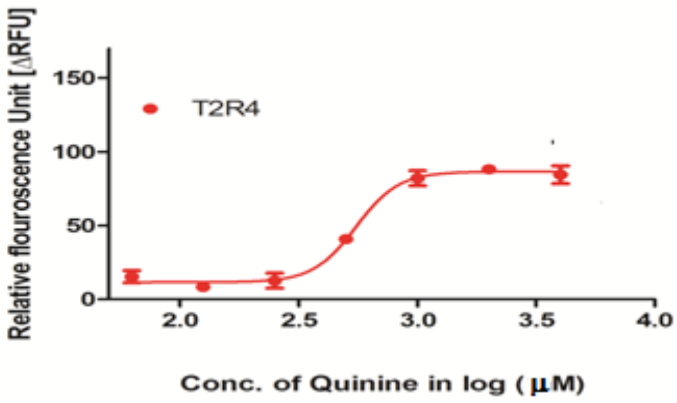

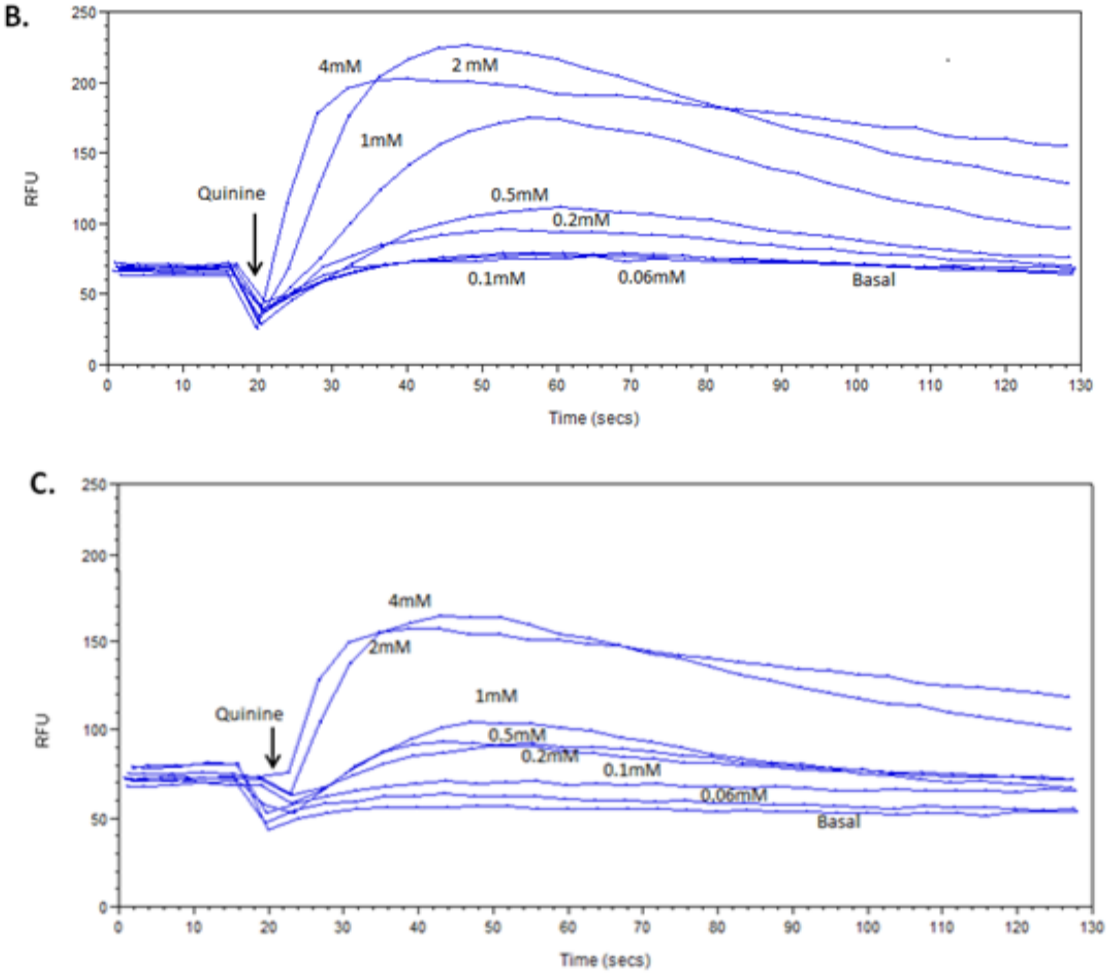

Figure 13. Concentration-dependent changes in intracellular calcium induced by quinine in HEK293T cell transiently transfected with T2R4. A. WT-T2R4 stimulated with different concentrations of quinine (0.06 mM to 4 mM) and the amount of calcium mobilized (ΔRFU) was measured using Fluo-4NW dye. Calcium mobilized (Δ RFU) was represented after subtracting the response from mock transfected cells (cells transfected with pcDNA 3.1 and Gα16/44). **B.** Representative calcium traces for HEK293T cells transiently transfected with T2R4 and stimulated with indicated quinine concentrations. **C.** Representative calcium traces for HEK293T cells with mock transfected (pcDNA) control.

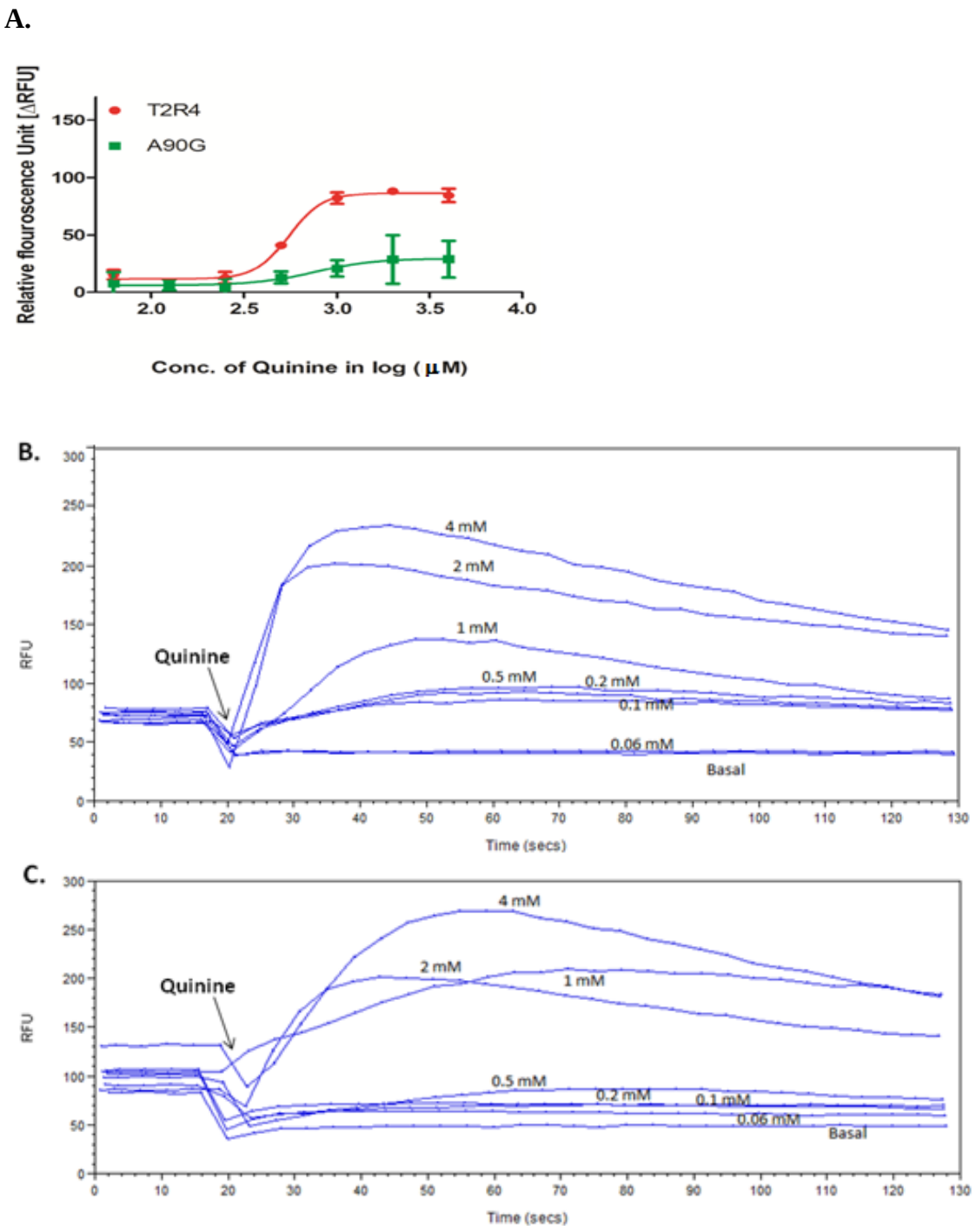

Figure 14. Concentration-dependent changes in intracellular calcium induced by quinine in HEK293T cell transiently transfected with A90G. A. A90G stimulated with different concentrations of quinine (0.06 mM to 4 mM) and the amount of calcium mobilized (ΔRFU) was measured using Fluo-4NW dye. Calcium mobilized (Δ RFU) was represented after subtracting the response from mock transfected cells (cells transfected with pcDNA 3.1 and Gα16/44). **B.** Representative calcium traces for HEK293T cells transiently transfected with A90G and stimulated with indicated quinine concentrations. **C.** Representative calcium traces for HEK293T cells with mock transfected (pcDNA) control.

A.

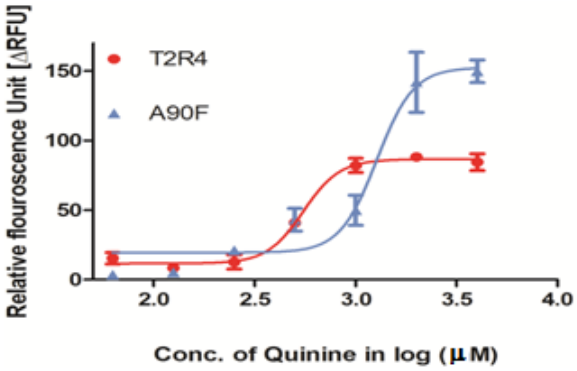

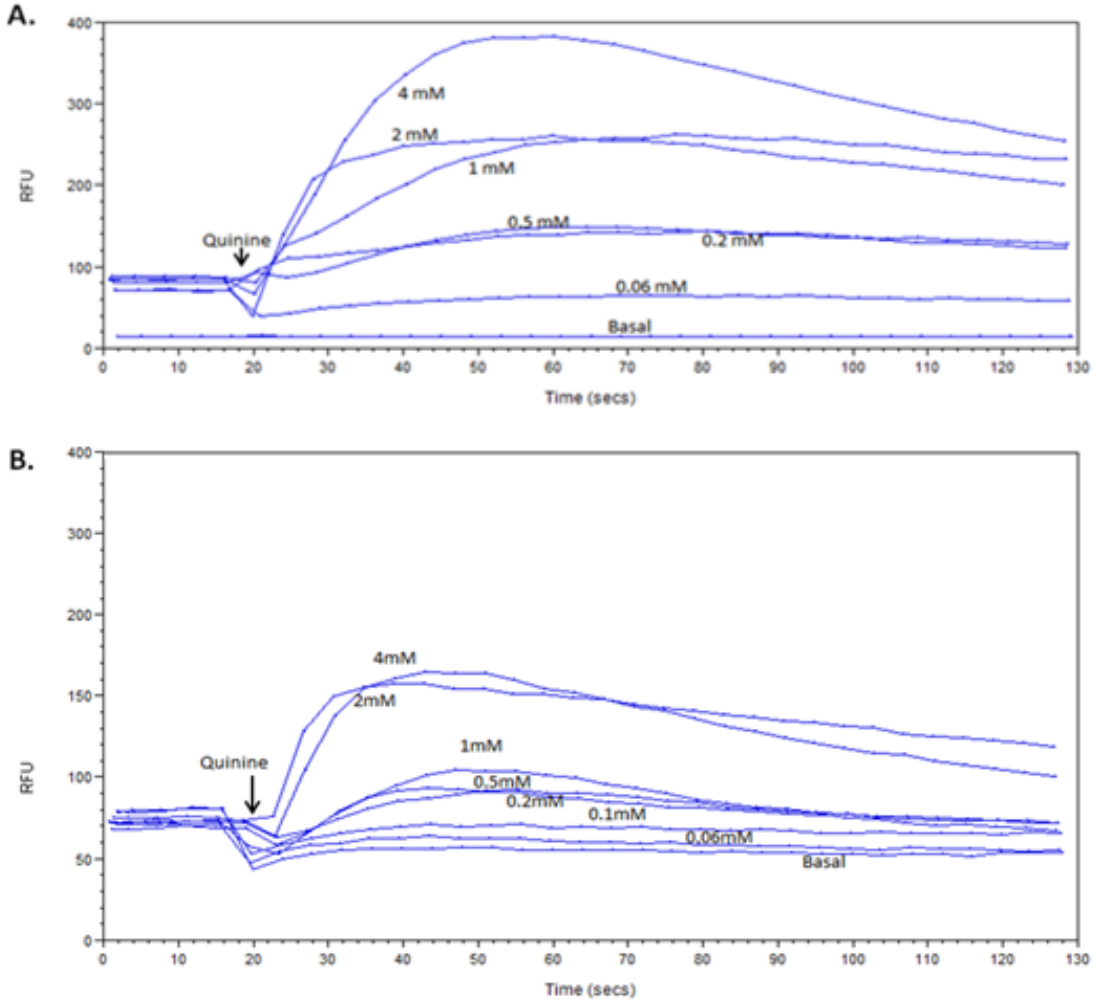

Figure 15. Concentration-dependent changes in intracellular calcium induced by quinine in HEK293T cell transiently transfected with A90F. A. A90F stimulated with different concentrations of quinine (0.06 mM to 4 mM) and the amount of calcium mobilized (ΔRFU) was measured using Fluo-4NW dye. Calcium mobilized (Δ RFU) was represented after subtracting the response from mock transfected cells (cells transfected with pcDNA 3.1 and Gα16/44). **B.** Representative calcium traces for HEK293T cells transiently transfected with A90F and stimulated with indicated quinine concentrations. **C.** Representative calcium traces for HEK293T cells with mock transfected (pcDNA) control.

A.

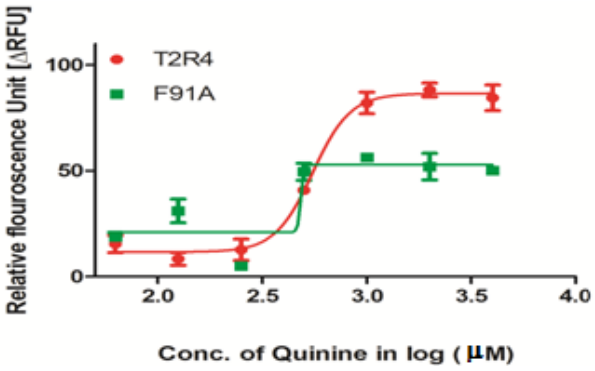

B.

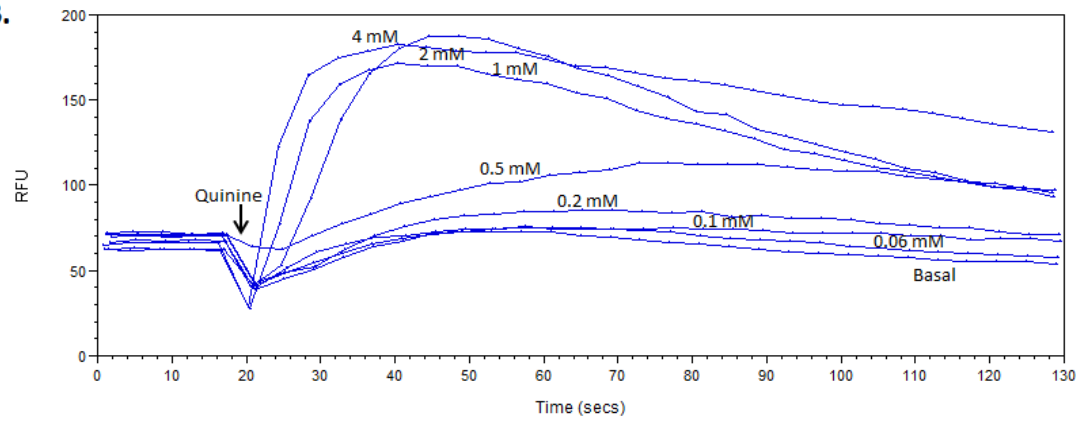

C.

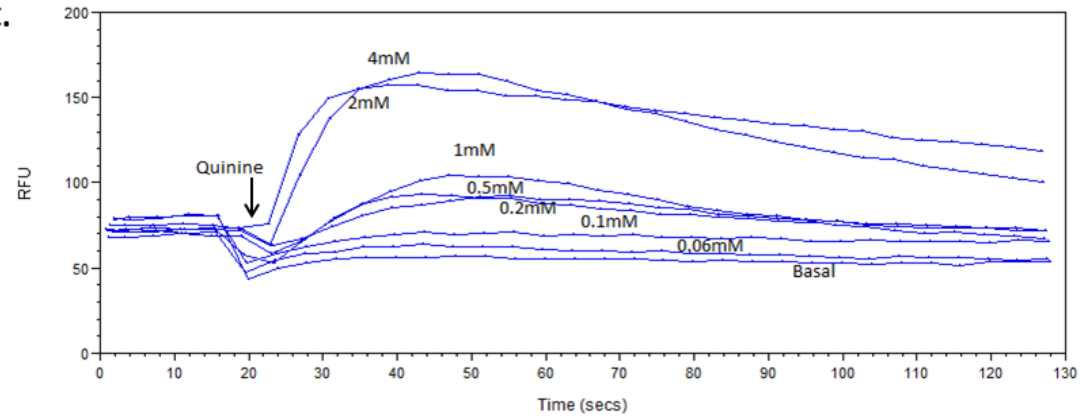

Figure 16. Concentration-dependent changes in intracellular calcium induced by quinine in HEK293T cell transiently transfected with F91A. A. F91A stimulated with different concentrations of quinine (0.06 mM to 4 mM) and the amount of calcium mobilized (ΔRFU) was measured using Fluo-4NW dye. Calcium mobilized (Δ RFU) was represented after subtracting the response from mock transfected cells (cells transfected with pcDNA 3.1 and Gα16/44). **B.** Representative calcium traces for HEK293T cells transiently transfected with F91A and stimulated with indicated quinine concentrations. **C.** Representative calcium traces for HEK293T cells with mock transfected (pcDNA) control.

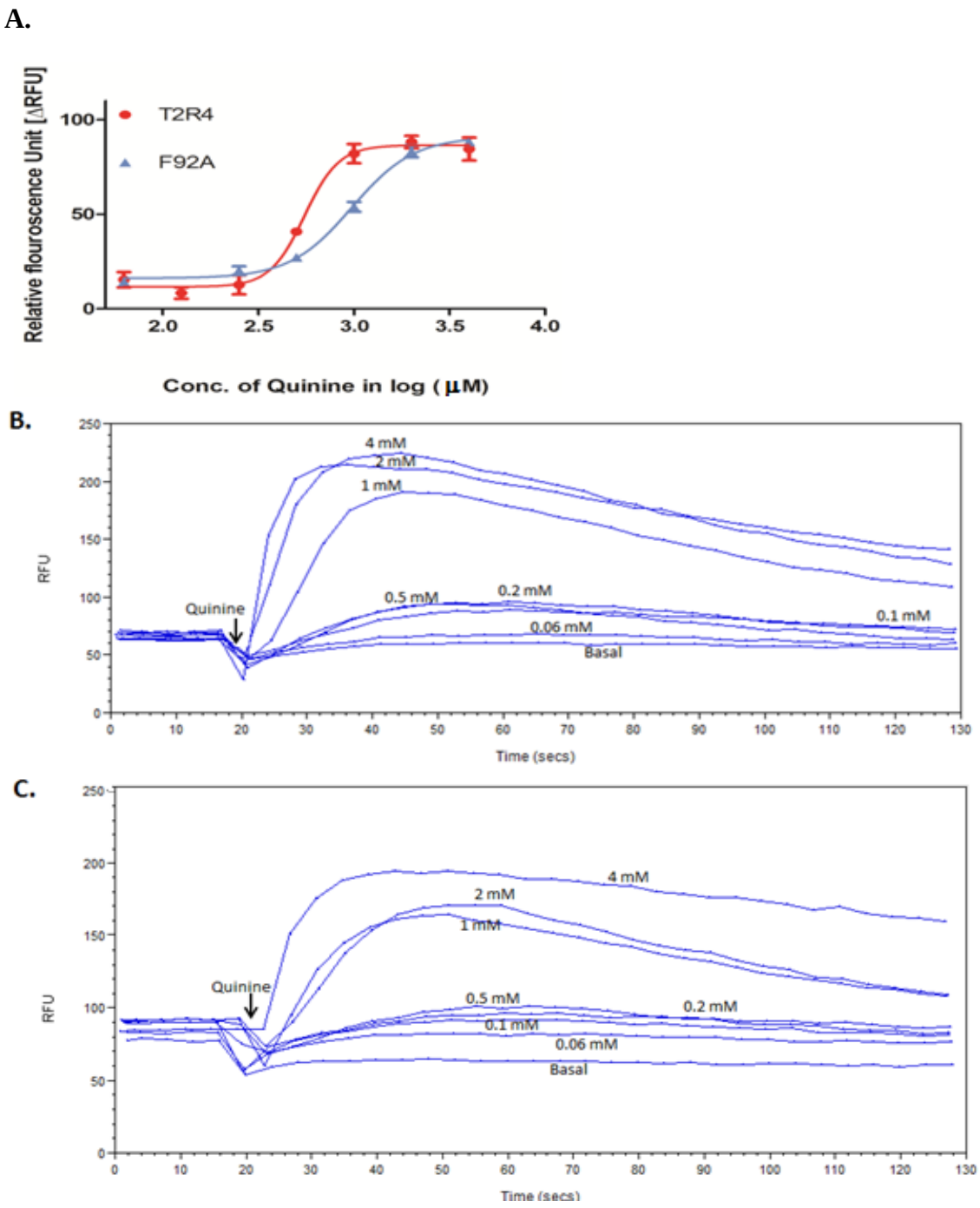

Figure 17. Concentration-dependent changes in intracellular calcium induced by quinine in HEK293T cell transiently transfected with F92A. A. F92A stimulated with different concentrations of quinine (0.06 mM to 4 mM) and the amount of calcium mobilized (ΔRFU) was measured using Fluo-4NW dye. Calcium mobilized (Δ RFU) was represented after subtracting the response from mock transfected cells (cells transfected with pcDNA 3.1 and Gα16/44). **B.** Representative calcium traces for HEK293T cells transiently transfected with F92A and stimulated with indicated quinine concentrations. **C.** Representative calcium traces for HEK293T cells with mock transfected (pcDNA) control.

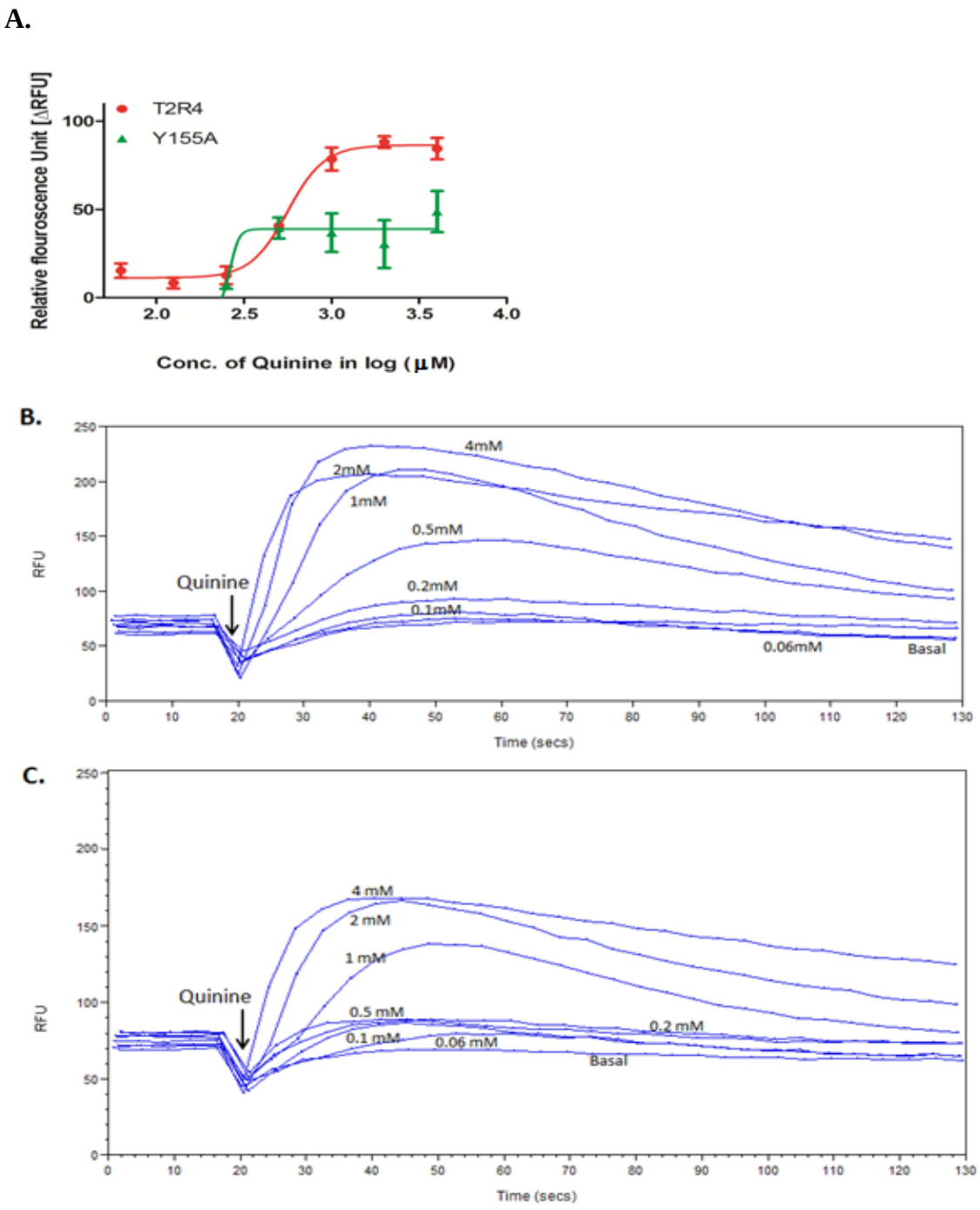

Figure 18. Concentration-dependent changes in intracellular calcium induced by quinine in HEK293T cell transiently transfected with Y155A. A. Y155A stimulated with different concentrations of quinine (0.06 mM to 4 mM) and the amount of calcium mobilized (ΔRFU) was measured using Fluo-4NW dye. Calcium mobilized (Δ RFU) was represented after subtracting the response from mock transfected cells (cells transfected with pcDNA 3.1 and Gα16/44). **B.** Representative calcium traces for HEK293T cells transiently transfected with Y155A and stimulated with indicated quinine concentrations. **C.** Representative calcium traces for HEK293T cells with mock transfected (pcDNA) control.

A.

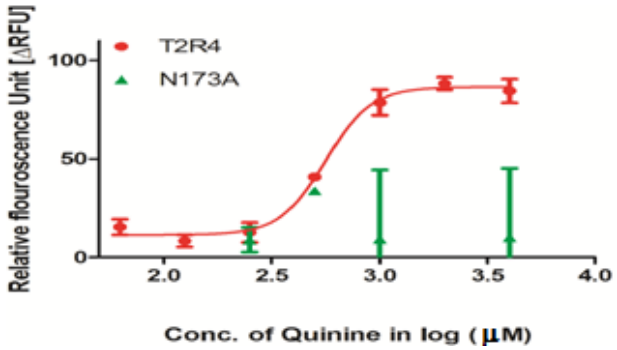

B.

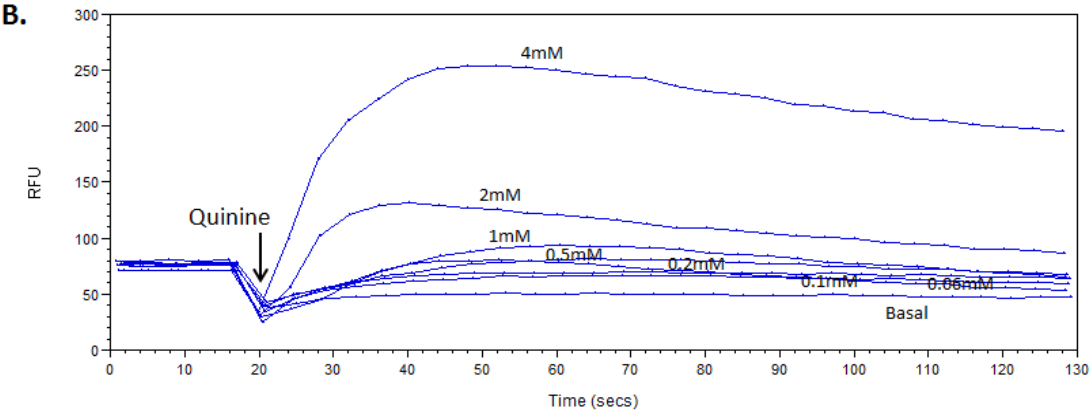

C.

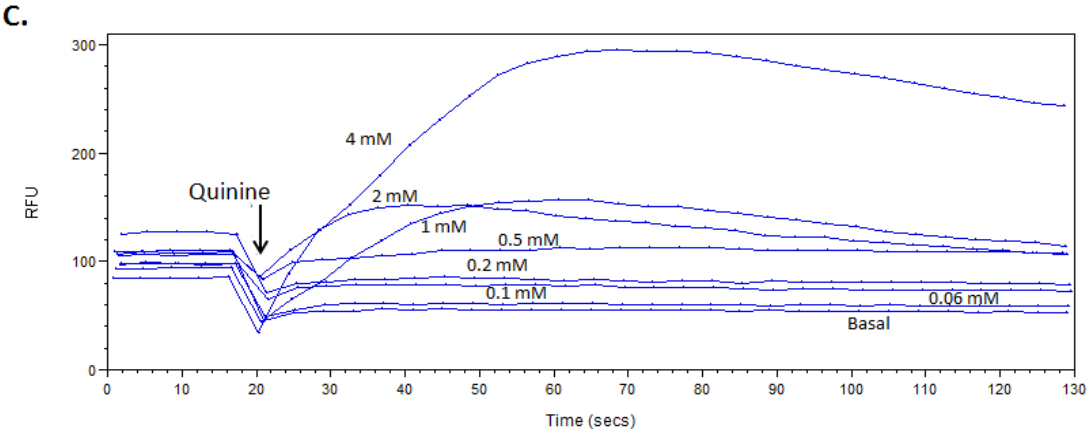

Figure 19. Concentration-dependent changes in intracellular calcium induced by quinine in HEK293T cell transiently transfected with N173A. A. N173A stimulated with different concentrations of quinine (0.06 mM to 4 mM) and the amount of calcium mobilized (ΔRFU) was measured using Fluo-4NW dye. Calcium mobilized (Δ RFU) was represented after subtracting the response from mock transfected cells (cells transfected with pcDNA 3.1 and Gα16/44). **B.** Representative calcium traces for HEK293T cells transiently transfected with N173A and stimulated with indicated quinine concentrations. **C.** Representative calcium traces for HEK293T cells with mock transfected (pcDNA) control.

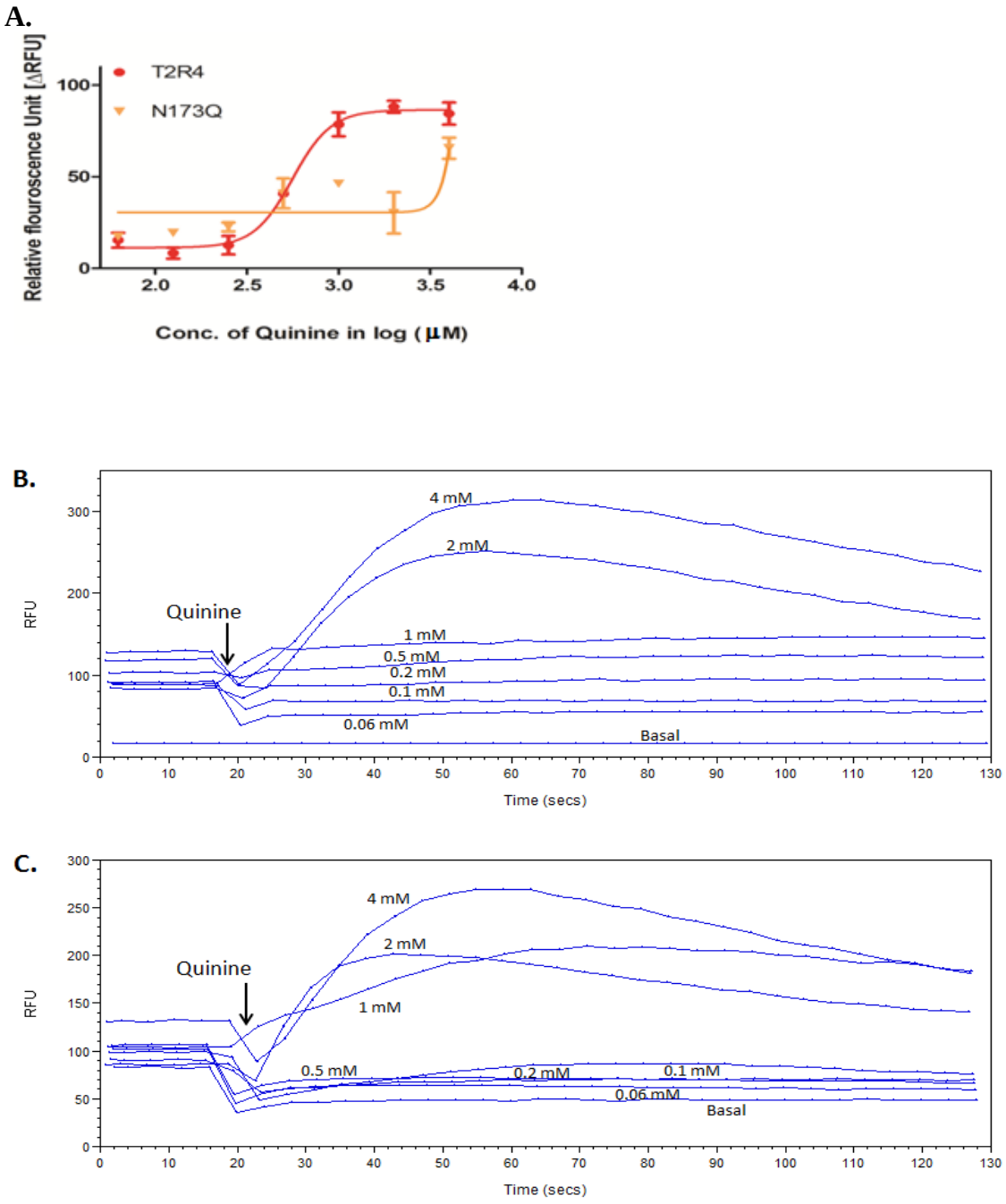

Figure 20. Concentration-dependent changes in intracellular calcium induced by quinine in HEK293T cell transiently transfected with N173Q. A. N173Q stimulated with different concentrations of quinine (0.06 mM to 4 mM) and the amount of calcium mobilized (ΔRFU) was measured using Fluo-4NW dye. Calcium mobilized (Δ RFU) was represented after subtracting the response from mock transfected cells (cells transfected with pcDNA 3.1 and Gα16/44). **B.** Representative calcium traces for HEK293T cells transiently transfected with N173Q and stimulated with indicated quinine concentrations. **C.** Representative calcium traces for HEK293T cells with mock transfected (pcDNA) control.

A.

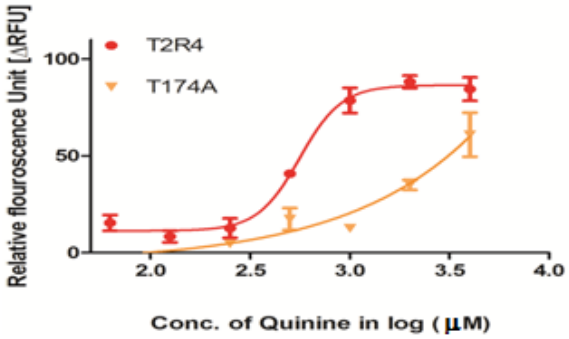

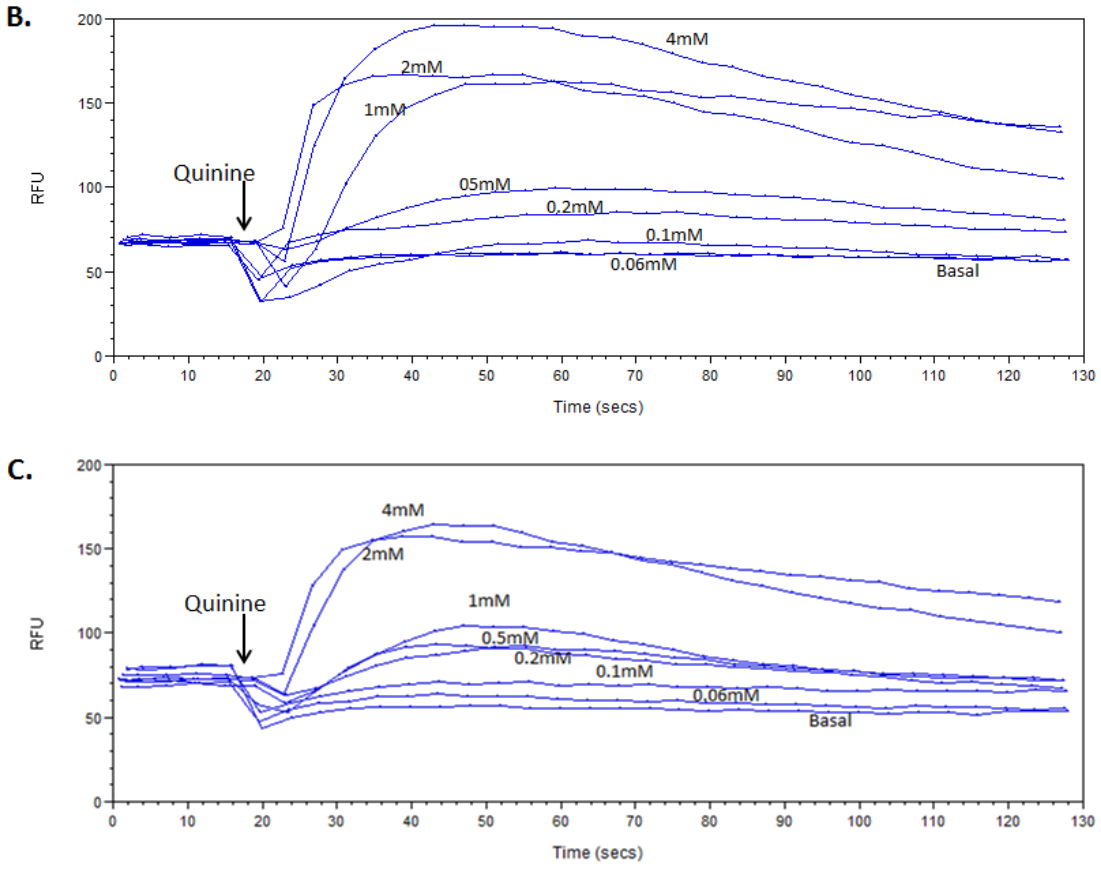

Figure 21. Concentration-dependent changes in intracellular calcium induced by quinine in HEK293T cell transiently transfected with T174A. A. T174A stimulated with different concentrations of quinine (0.06 mM to 4 mM) and the amount of calcium mobilized (ΔRFU) was measured using Fluo-4NW dye. Calcium mobilized (Δ RFU) was represented after subtracting the response from mock transfected cells (cells transfected with pcDNA 3.1 and Gα16/44). **B.** Representative calcium traces for HEK293T cells transiently transfected with T174A and stimulated with indicated quinine concentrations. **C.** Representative calcium traces for HEK293T cells with mock transfected (pcDNA) control.

A.

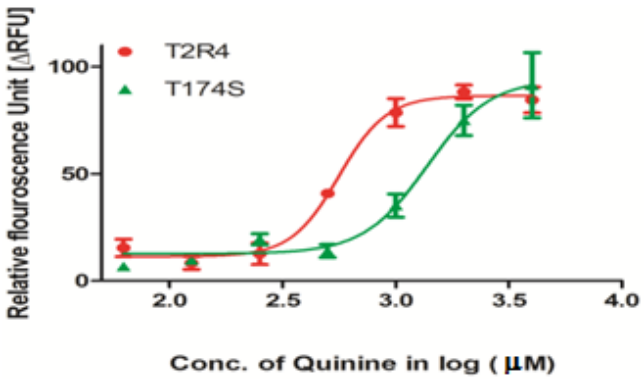

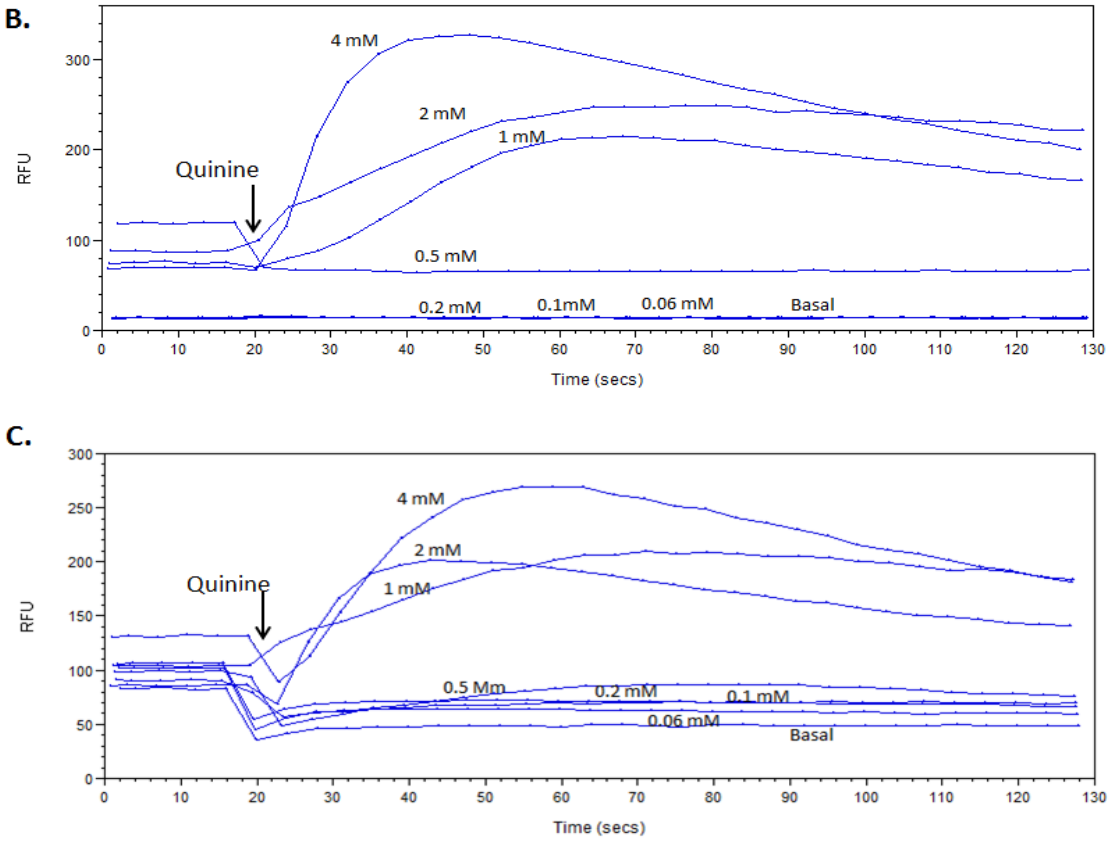

Figure 22. Concentration-dependent changes in intracellular calcium induced by quinine in HEK293T cell transiently transfected with T174S. A. T174S stimulated with different concentrations of quinine (0.06 mM to 4 mM) and the amount of calcium mobilized (ΔRFU) was measured using Fluo-4NW dye. Calcium mobilized (Δ RFU) was represented after subtracting the response from mock transfected cells (cells transfected with pcDNA 3.1 and Gα16/44). **B.** Representative calcium traces for HEK293T cells transiently transfected with T174S and stimulated with indicated quinine concentrations. **C.** Representative calcium traces for HEK293T cells with mock transfected (pcDNA) control.

A.

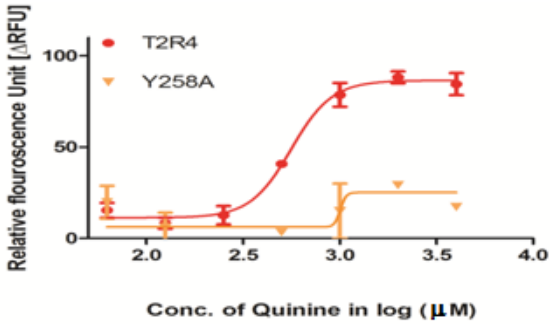

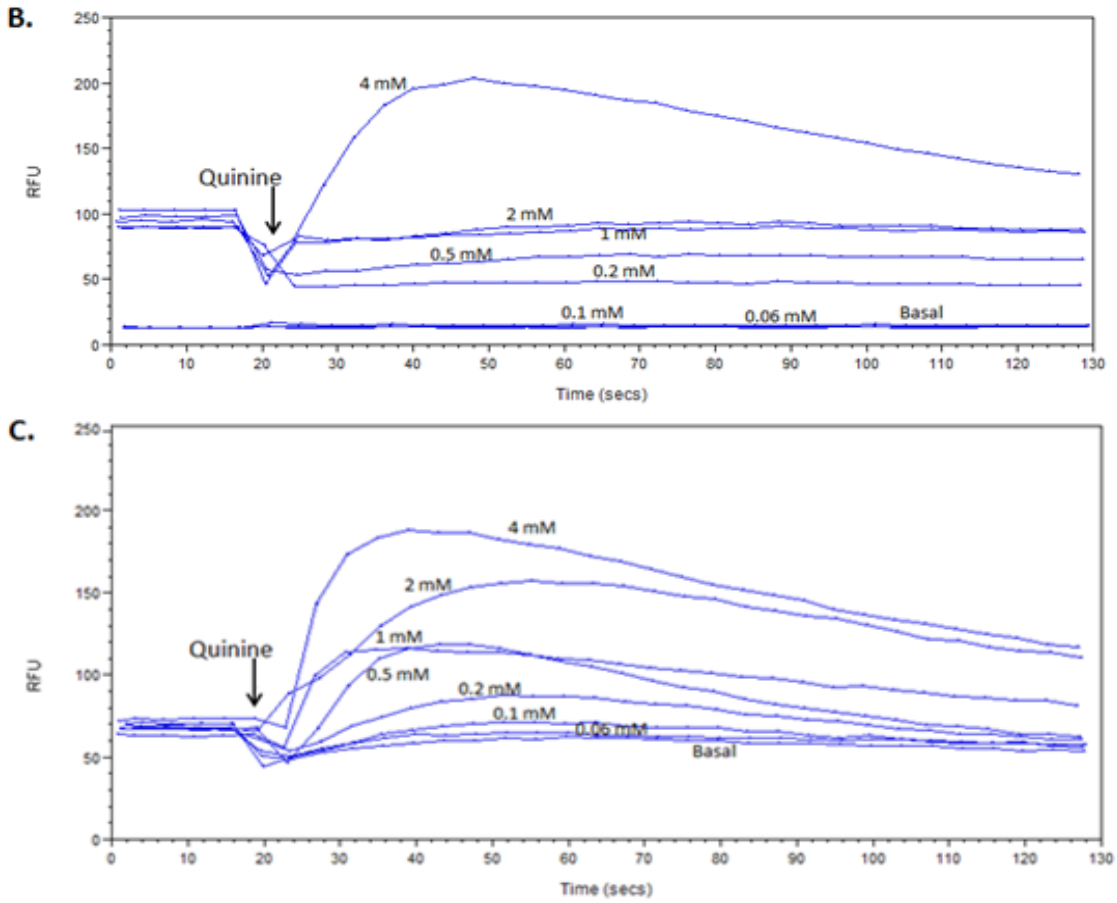

Figure 23. Concentration-dependent changes in intracellular calcium induced by quinine in HEK293T cell transiently transfected with Y258A. A. Y258A stimulated with different concentrations of quinine (0.06 mM to 4 mM) and the amount of calcium mobilized (ΔRFU) was measured using Fluo-4NW dye. Calcium mobilized (Δ RFU) was represented after subtracting the response from mock transfected cells (cells transfected with pcDNA 3.1 and Gα16/44). **B.** Representative calcium traces for HEK293T cells transiently transfected with Y258A and stimulated with indicated quinine concentrations. **C.** Representative calcium traces for HEK293T cells with mock transfected (pcDNA) control.

A.

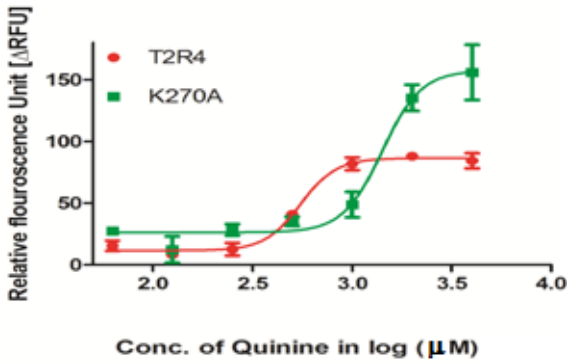

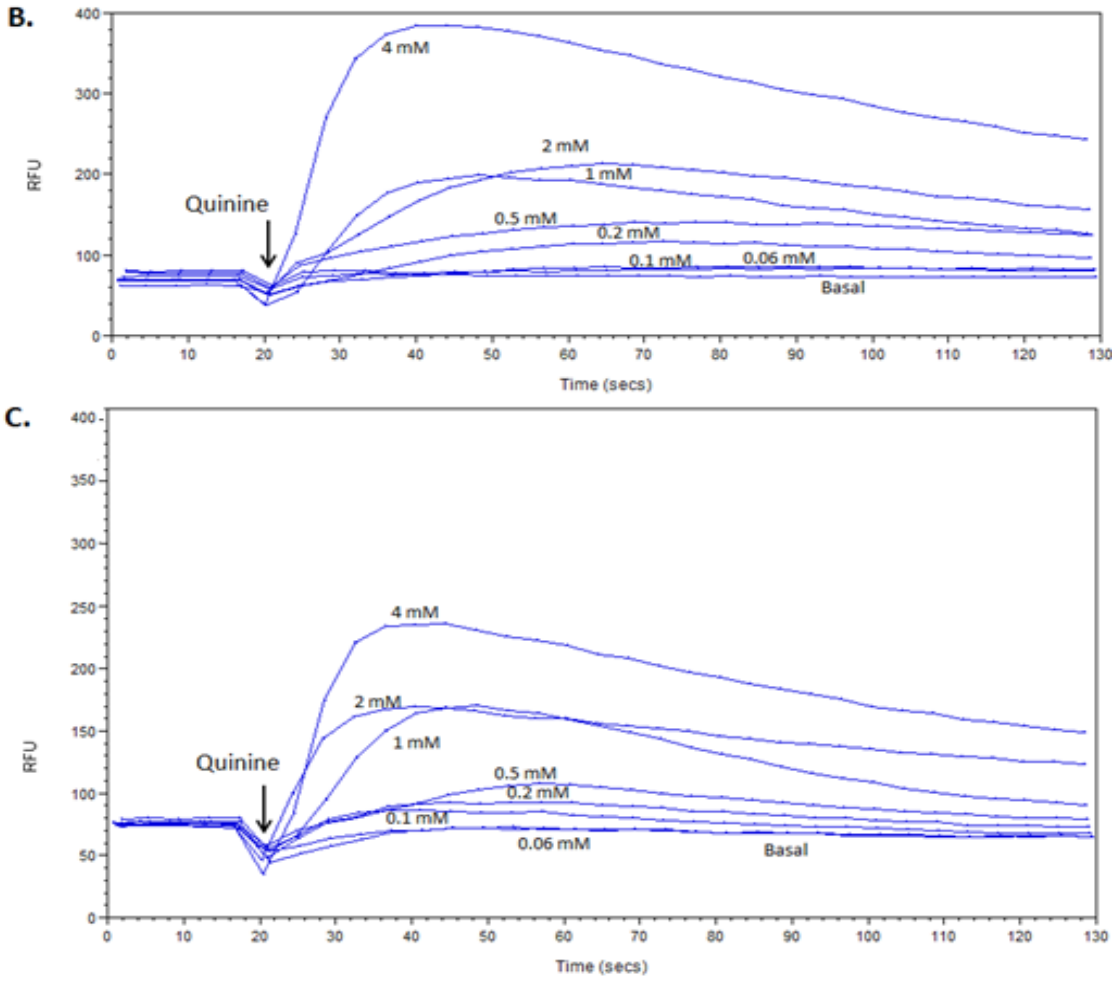

Figure 24. Concentration-dependent changes in intracellular calcium induced by quinine in HEK293T cell transiently transfected with K270A. A. K270A stimulated with different concentrations of quinine (0.06 mM to 4 mM) and the amount of calcium mobilized (ΔRFU) was measured using Fluo-4NW dye. Calcium mobilized (Δ RFU) was represented after subtracting the response from mock transfected cells (cells transfected with pcDNA 3.1 and Gα16/44). **B.** Representative calcium traces for HEK293T cells transiently transfected with K270A and stimulated with indicated quinine concentrations. **C.** Representative calcium traces for HEK293T cells with mock transfected (pcDNA) control.

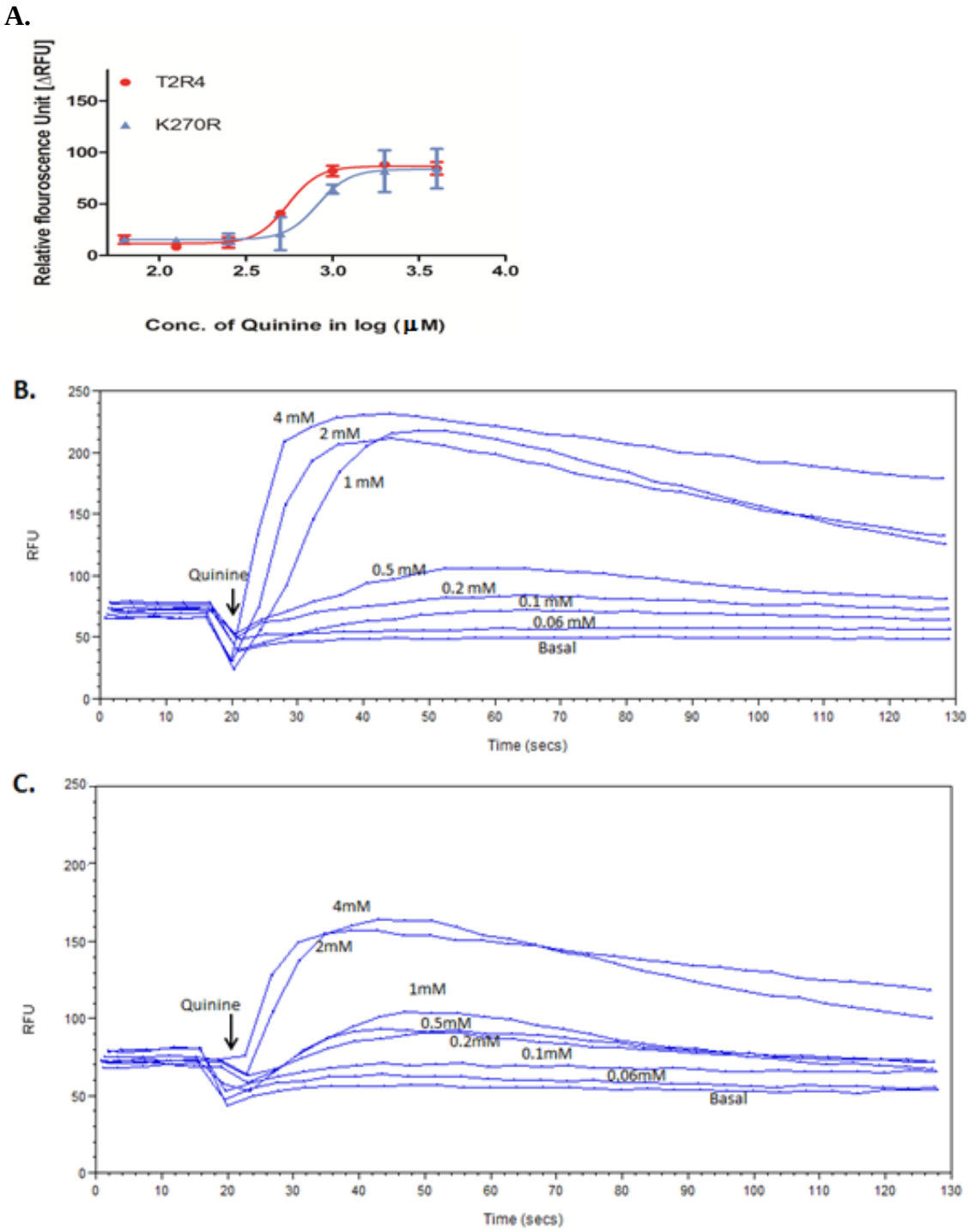

Figure 25. Concentration-dependent changes in intracellular calcium induced by quinine in HEK293T cell transiently transfected with K270R. A. K270R stimulated with different concentrations of quinine (0.06 mM to 4 mM) and the amount of calcium mobilized (ΔRFU) was measured using Fluo-4NW dye. Calcium mobilized (Δ RFU) was represented after subtracting the response from mock transfected cells (cells transfected with pcDNA 3.1 and Gα16/44). **B.** Representative calcium traces for HEK293T cells transiently transfected with K270R and stimulated with indicated quinine concentrations. **C.** Representative calcium traces for HEK293T cells with mock transfected (pcDNA) control.

CHAPTER FIVE

DISCUSSION AND CONCLUSION

Within the GPCR families and subfamilies, there is a remarkable diversity in the location, shape, and features of the ligand binding pocket. For example, in Class A GPCRs, the ligand binds within a pocket that is lined by amino acids from the ECLs and extracellular side of TM regions (Chakraborty et al. 2012). However, in Class C GPCRs including metabotropic glutamate receptors or mGluRs and T1Rs, the ligand binds to the N-terminal domain also referred to as the venus fly-trap domain. Similar to other GPCRs, T2Rs have the ability to bind to ligands of diverse chemical properties, shapes, and sizes. To understand the receptor-agonist interactions, different research groups have used a combination of *in silico* and experimental methods.

Since some of the T2R ligands are small, they were hypothesized to bind deep within the TM core. However, there is growing evidence suggesting the role of ECLs in the ligand binding in T2Rs. Swapping of ECL1 between T2R43 and T2R44 showed defective agonist binding when the T2R43 chimera was stimulated with its agonist n-isopropyl-2-methyl-5-nitrobenzenesulfonamide (Pronin et al. 2004). In most of the T2Rs, TM3 plays a crucial role in ligand binding (Behrens and Meyerhof 2013, Biarnes et al. 2010, Brockhoff et al. 2010, Sakurai et al. 2010a, Sakurai et al. 2010b, Upadhyaya et al. 2010).

In this structure-function study, the quinine-binding pocket of the moderately tuned T2R4 was elucidated. Molecular docking studies suggest that quinine binds to T2R4 towards the extracellular side of the receptor with contributions from amino acids on TM3-TM4-TM6-TM7 and ECLs2 and 3. The ligand-binding pocket of T2R4 for quinine is

hydrophilic in nature. Twelve point mutations were generated at eight positions in T2R4 to understand the nature and importance of these residues in agonist binding.

5.1 TM3 mutants

In T2R4, three residues A90, F91 and F92 from TM3, are part of the ligand-binding pocket. A90 is found to be important for ligand binding, backbone of alanine forming H-bond with quinine. Mutation of this residue significantly affected ligand binding. In the same vicinity, in other T2Rs like T2R16 (Sakurai et al. 2010b), T2R30 (Pronin et al. 2004), T2R38 (Biarnes et al. 2010) and T2R46 (Brockhoff et al. 2010), an asparagine is present and it is crucial for ligand binding. However, there is no asparagine on the extracellular side of TM3 in T2R4. This confirms the diversity in the ligand-binding pocket of these residues.

Molecular modeling studies showed that A90 is forming a backbone contact with N-group on the quinoline ring. Alanine is a non-polar amino acid consisting of only a methyl side chain, whereas glycine is a very small amino acid without a functional side chain. FACS data showed that the cell surface expression of the A90G mutant was similar to that of WT-T2R4. However, there was no intracellular calcium mobilization when stimulated with quinine. In TM regions, glycine because of its small size helps in helical packing of GPCRs. With the A90G mutation, there is no problem with helical packing as the expression of this mutant was similar to WT-T2R4. However, the mutation led to loss of crucial contact between the backbone of glycine with the N-atom of quinolone ring, resulting in loss of function. Interestingly, with the A90F mutation, the expression was reduced by 30% due to the bulky aromatic ring of phenylalanine interfering with the helix packing. Surprisingly, the functional response was enhanced and the A90F showed hyperactivity. The F91A showed no quinine-concentration dependent increase in calcium

mobilization though it was expressed at levels similar to WT-T2R4, while F92A showed a functional response similar to WT-T2R4. More mutations might be needed at A90 and F91, such as an A90Y or F91Y to elucidate the reasons for the hyperactivity of A90F, and loss of function of F91A mutant.

5.2 TM4 mutant

The only residue from TM4 involved in ligand binding was Y155. Molecular modeling suggested pi-pi interactions between the quinoline ring of quinine and aromatic ring of tyrosine. In the Y155A mutation, these interactions between the receptor and ligand were lost and resulted in the loss of function.

5.3 ECL2 mutants

Based on molecular modeling, two residues N173 and T174 from ECL2 region were involved in H-bond with the hydroxyl group of quinine. N173 was mutated to alanine (N173A), and to a functionally similar residue glutamine (N173Q). Both mutants, N173A and N173Q showed similar cell surface expression compared to WT-T2R4. However, no functional response was seen for both the mutants. It suggests that N173 is essential for binding to quinine, and both length of the side chain (compared to asparagine, glutamine as an additional –CH2 group in its side chain), and H-bond capability at position 173 is crucial.

The next ECL2 residue characterized was T174. In the molecular model, the side chain of threonine was interacting with quinine. T174A mutant was generated to eliminate the side chain of threonine, thereby affecting the coordination through H-bonding. Functional characterization of this mutant showed no concentration dependent calcium mobilization, while flow cytometry showed similar cell surface expression as that of WT-

T2R4. To further characterize the importance of H-bond at this position, T174S was generated. Functional characterization of this mutant showed a 2.5-fold increased EC_{50} value than WT-T2R4. This suggests that for ligand interaction at this position, in addition to H-bond formation, additional characteristics and conformation of the amino acid side chain also play a role.

5.4 TM6-ECL3-TM7 mutants

The next important residue involved in ligand binding was Y258, present at the interface of TM6-ECL3. Based on molecular modeling, quinoline ring of quinine was packed between Y155 and Y258. The Y258A mutant showed complete loss of quinine induced calcium mobilization. The Y258 along with Y155 play an essential role in interaction with the quinoline ring of quinine. The last residue characterized in the ligand-binding pocket was K270, present at the interface of ECL3-TM7. Two mutations K270A and K270R were generated at this position. K270A showed 30% reduction in cell surface expression, whereas K270R showed similar cell surface expression as WT-T2R4. Interestingly, the K270A displayed hyperactivity, while the complementary mutant, K270R displayed similar function as WT-T2R4. In the molecular docking studies no direct H-bonding interactions were observed between the quinine and K270. However, mutational studies suggest that a positively charged residue might be important at this position. This residue may have indirect effect on the ligand-binding pocket by influencing the other residues.

5.5 Conclusion and future directions

In humans, of the 25 T2Rs, 20 have been deorphanized (ligands known) thus far. Some human T2Rs, including T2R4 bind to more than 10 bitter compounds. However, the ligand pose/binding mode and receptor specificity were least understood. In this study, a combination of approaches that involve molecular modeling and site-directed mutagenesis was used to identify the amino acid residues important for quinine binding in T2R4. This study identified that quinine binds to the extracellular side of T2R4, and not deep within the TM core. In addition, the following amino acids A90, F91, Y155, N173, T174, Y258 and K270 amino acids play an important role in quinine binding to T2R4. The detailed study of residues interacting with ligand will help in understanding how various ligands interact with T2Rs, and facilitate the pharmacological and sensory characterization of potent antagonists or bitter taste blockers. The characterization of novel ligands, including bitter taste blockers will help in dissecting the signaling mechanism(s) of T2Rs.

CHAPTER SIX

REFERENCES

Adler E, Hoon MA, Mueller KL, Chandrashekar J, Ryba NJ, Zuker CS. 2000. A novel family of mammalian taste receptors. Cell 100: 693-702.

An SS, Wang WC, Koziol-White CJ, Ahn K, Lee DY, Kurten RC, Panettieri RA, Jr., Liggett SB. 2012. TAS2R activation promotes airway smooth muscle relaxation despite beta(2)-adrenergic receptor tachyphylaxis. Am J Physiol Lung Cell Mol Physiol 303: L304-311.

Bachmanov AA BG. 2007. Taste receptor genes. Annu Review of Nutrition: 389-414.

Beauchamp GK. 1995. Chemical Signals and Repellency: Problems and Prognosis.

Behrens M, Meyerhof W. 2009. Mammalian bitter taste perception. Results Probl Cell Differ 47: 203-220.

Behrens M, Meyerhof W.. 2013. Bitter taste receptor research comes of age: from characterization to modulation of TAS2Rs. Semin Cell Dev Biol 24: 215-221.

Behrens M, Brockhoff A, Kuhn C, Bufe B, Winnig M, Meyerhof W. 2004. The human taste receptor hTAS2R14 responds to a variety of different bitter compounds. Biochem Biophys Res Commun 319: 479-485.

Beidler LM, Smallman RL. 1965. Renewal of cells within taste buds. J Cell Biol 27: 263-272.

Belitz H-D WH. 1985. Bitter compounds: occurrence and structure-activity relationship. Food rev Int 1: 271-354.

Biarnes X, Marchiori A, Giorgetti A, Lanzara C, Gasparini P, Carloni P, Born S, Brockhoff A, Behrens M, Meyerhof W. 2010. Insights into the binding of Phenyltiocarbamide (PTC) agonist to its target human TAS2R38 bitter receptor. PLoS One 5: e12394.

Birnbaumer L, Abramowitz J, Brown AM. 1990. Receptor-effector coupling by G proteins. Biochim Biophys Acta 1031: 163-224.

Born S, Levit A, Niv MY, Meyerhof W, Behrens M. 2013. The human bitter taste receptor TAS2R10 is tailored to accommodate numerous diverse ligands. J Neurosci 33: 201-213.

Brockhoff A, Behrens M, Niv MY, Meyerhof W. 2010. Structural requirements of bitter taste receptor activation. Proc Natl Acad Sci U S A 107: 11110-11115.

Brockhoff A, Behrens M, Massarotti A, Appendino G, Meyerhof W. 2007. Broad tuning of the human bitter taste receptor hTAS2R46 to various sesquiterpene lactones, clerodane and labdane diterpenoids, strychnine, and denatonium. J Agric Food Chem 55: 6236-6243.

Caicedo A, Kim KN, Roper SD. 2002. Individual mouse taste cells respond to multiple chemical stimuli. J Physiol 544: 501-509.

Chakraborty R, Pydi SP, Gleim S, Dakshinamurti S, Hwa J, Chelikani P. 2012. Site-Directed Mutations and the Polymorphic Variant Ala160Thr in the Human Thromboxane Receptor Uncover a Structural Role for Transmembrane Helix 4. PLoS One 7: e29996.

Chandrashekar J, Mueller KL, Hoon MA, Adler E, Feng L, Guo W, Zuker CS, Ryba NJ. 2000. T2Rs function as bitter taste receptors. Cell 100: 703-711.

Chen X, Gabitto M, Peng Y, Ryba NJ, Zuker CS. 2011. A gustotopic map of taste qualities in the mammalian brain. Science 333: 1262-1266.

Chothia C, Lesk AM. 1986. The relation between the divergence of sequence and structure in proteins. EMBO J 5: 823-826.

Clapp TR, Stone LM, Margolskee RF, Kinnamon SC. 2001. Immunocytochemical evidence for co-expression of Type III IP3 receptor with signaling components of bitter taste transduction. BMC Neurosci 2: 6.

Conte C, Ebeling M, Marcuz A, Nef P, Andres-Barquin PJ. 2002. Identification and characterization of human taste receptor genes belonging to the TAS2R family. Cytogenet Genome Res 98: 45-53.

Conte C, Ebeling M, Marcuz A, Nef P, Andres-Barquin PJ. 2003. Evolutionary relationships of the Tas2r receptor gene families in mouse and human. Physiol Genomics 14: 73-82.

Deshpande DA, Wang WC, McIlmoyle EL, Robinett KS, Schillinger RM, An SS, Sham JS, Liggett SB. 2010. Bitter taste receptors on airway smooth muscle bronchodilate by localized calcium signaling and reverse obstruction. Nat Med 16: 1299-1304.

Dotson CD, et al. 2008. Bitter taste receptors influence glucose homeostasis. PLoS One 3: e3974.

DuBois GE DJ, Lally V. 2008. chemistry of gustatory stimuli olfaction and taste: 27-74.

Erickson RP. 2000. The evolution of neural coding ideas in the chemical senses. Physiol Behav 69: 3-13.

Finger TE, Bottger B, Hansen A, Anderson KT, Alimohammadi H, Silver WL. 2003. Solitary chemoreceptor cells in the nasal cavity serve as sentinels of respiration. Proc Natl Acad Sci U S A 100: 8981-8986.

Ganchrow JG, JR); Steiner, JE (Steiner, JE); Daher, M (Daher, M). 1983. Neonatal facial expressions in response to different qualities and intensities of gustatory stimuli. INFANT BEHAVIOR & DEVELOPMENT 6: 189-200

Gasparini F, Kuhn R, Pin JP. 2002. Allosteric modulators of group I metabotropic glutamate receptors: novel subtype-selective ligands and therapeutic perspectives. Curr Opin Pharmacol 2: 43-49.

Gilbertson TA, Avenet P, Kinnamon SC, Roper SD. 1992. Proton currents through amiloride-sensitive Na channels in hamster taste cells. Role in acid transduction. J Gen Physiol 100: 803-824.

Hoon MA, Adler E, Lindemeier J, Battey JF, Ryba NJ, Zuker CS. 1999. Putative mammalian taste receptors: a class of taste-specific GPCRs with distinct topographic selectivity. Cell 96: 541-551.

Ishimaru Y, Matsunami H. 2009. Transient receptor potential (TRP) channels and taste sensation. J Dent Res 88: 212-218.

Ishimaru Y, Inada H, Kubota M, Zhuang H, Tominaga M, Matsunami H. 2006. Transient receptor potential family members PKD1L3 and PKD2L1 form a candidate sour taste receptor. Proc Natl Acad Sci U S A 103: 12569-12574.

Janssen S, Laermans J, Verhulst PJ, Thijs T, Tack J, Depoortere I. 2011. Bitter taste receptors and alpha-gustducin regulate the secretion of ghrelin with functional effects on food intake and gastric emptying. Proc Natl Acad Sci U S A 108: 2094-2099.

Jeon TI, Zhu B, Larson JL, Osborne TF. 2008. SREBP-2 regulates gut peptide secretion through intestinal bitter taste receptor signaling in mice. J Clin Invest 118: 3693-3700.

Katz DB, Nicolelis MA, Simon SA. 2000. Nutrient tasting and signaling mechanisms in the gut. IV. There is more to taste than meets the tongue. Am J Physiol Gastrointest Liver Physiol 278: G6-9.

Kim UK, Breslin PA, Reed D, Drayna D. 2004. Genetics of human taste perception. J Dent Res 83: 448-453.

Kroeze WK, Sheffler DJ, Roth BL. 2003. G-protein-coupled receptors at a glance. J Cell Sci 116: 4867-4869.

Kuhn C, Bufe B, Batram C, Meyerhof W. 2010. Oligomerization of TAS2R bitter taste receptors. Chem Senses 35: 395-406.

Lagerstrom MC, Schioth HB. 2008. Structural diversity of G protein-coupled receptors and significance for drug discovery. Nat Rev Drug Discov 7: 339-357.

Lawton DM, Furness DN, Lindemann B, Hackney CM. 2000. Localization of the glutamate-aspartate transporter, GLAST, in rat taste buds. Eur J Neurosci 12: 3163-3171.

Le Neve B, Foltz M, Daniel H, Gouka R. 2010. The steroid glycoside H.g.-12 from Hoodia gordonii activates the human bitter receptor TAS2R14 and induces CCK release from HuTu-80 cells. Am J Physiol Gastrointest Liver Physiol 299: G1368-1375.

Li X, Staszewski L, Xu H, Durick K, Zoller M, Adler E. 2002. Human receptors for sweet and umami taste. Proc Natl Acad Sci U S A 99: 4692-4696.

Lindemann B. 2001. Receptors and transduction in taste. Nature 413: 219-225.

Maehashi K, Huang L. 2009. Bitter peptides and bitter taste receptors. Cell Mol Life Sci 66: 1661-1671.

Margolskee RF. 2002. Molecular mechanisms of bitter and sweet taste transduction. J Biol Chem 277: 1-4.

Mbiene JP, Maccallum DK, Mistretta CM. 1997. Organ cultures of embryonic rat tongue support tongue and gustatory papilla morphogenesis in vitro without intact sensory ganglia. J Comp Neurol 377: 324-340.

McLaughlin SK, McKinnon PJ, Margolskee RF. 1992. Gustducin is a taste-cell-specific G protein closely related to the transducins. Nature 357: 563-569.

Meyerhof W, Batram C, Kuhn C, Brockhoff A, Chudoba E, Bufe B, Appendino G, Behrens M. 2010. The molecular receptive ranges of human TAS2R bitter taste receptors. Chem Senses 35: 157-170.

Nelson G, Hoon MA, Chandrashekar J, Zhang Y, Ryba NJ, Zuker CS. 2001. Mammalian sweet taste receptors. Cell 106: 381-390.

Nelson G, Chandrashekar J, Hoon MA, Feng L, Zhao G, Ryba NJ, Zuker CS. 2002. An amino-acid taste receptor. Nature 416: 199-202.

Nelson GM, Finger TE. 1993. Immunolocalization of different forms of neural cell adhesion molecule (NCAM) in rat taste buds. J Comp Neurol 336: 507-516.

Northcutt RG. 2004. Taste Buds: Development and Evolution. Brain Behav Evol Vol. 64, No. 3: 198–206

Palmer LG. 1987. Ion selectivity of epithelial Na channels. J Membr Biol 96: 97-106.

Pfaffmann C. 1959. The sense of taste. American Physiological Society 1: 507-533.

Pin JP, Galvez T, Prezeau L. 2003. Evolution, structure, and activation mechanism of family 3/C G-protein-coupled receptors. Pharmacol Ther 98: 325-354.

Pronin AN, Tang H, Connor J, Keung W. 2004. Identification of ligands for two human bitter T2R receptors. Chem Senses 29: 583-593.

Pydi S, Singh N, Upadhyaya J, Bhullar RP, Chelikani P. 2014. The third intracellular loop plays a critical role in bitter taste receptor activation. Biochim Biophys Acta 1838: 231-236.

Pydi SP, Bhullar RP, Chelikani P. 2012. Constitutively active mutant gives novel insights into the mechanism of bitter taste receptor activation. J Neurochem 122: 537-544.

Pydi SP, Chakraborty R, Bhullar RP, Chelikani P. 2013. Role of rhodopsin N-terminus in structure and function of rhodopsin-bitter taste receptor chimeras. Biochem Biophys Res Commun 430: 179-182.

Roper SD. 2007. Signal transduction and information processing in mammalian taste buds. Pflugers Arch 454: 759-776.

Sakurai T, Misaka T, Ueno Y, Ishiguro M, Matsuo S, Ishimaru Y, Asakura T, Abe K. 2010a. The human bitter taste receptor, hTAS2R16, discriminates slight differences in the configuration of disaccharides. Biochem Biophys Res Commun 402: 595-601.

Sakurai T, et al. 2010b. Characterization of the beta-D-glucopyranoside binding site of the human bitter taste receptor hTAS2R16. J Biol Chem 285: 28373-28378.

Shah AS, Ben-Shahar Y, Moninger TO, Kline JN, Welsh MJ. 2009. Motile cilia of human airway epithelia are chemosensory. Science 325: 1131-1134.

Shi P, Zhang J, Yang H, Zhang YP. 2003. Adaptive diversification of bitter taste receptor genes in Mammalian evolution. Mol Biol Evol 20: 805-814.

Singh N, Vrontakis M, Parkinson F, Chelikani P. 2011a. Functional bitter taste receptors are expressed in brain cells. Biochem Biophys Res Commun 406: 146-151.

Singh N, Pydi SP, Upadhyaya J, Chelikani P. 2011b. Structural Basis of Activation of Bitter Taste Receptor T2R1 and Comparison with Class A G-protein-coupled Receptors (GPCRs). J Biol Chem 286: 36032-36041.

Smith DV, St John SJ. 1999. Neural coding of gustatory information. Curr Opin Neurobiol 9: 427-435.

Smith DV, John SJ, Boughter JD. 2000. Neuronal cell types and taste quality coding. Physiol Behav 69: 77-85.

Upadhyaya J, Pydi SP, Singh N, Aluko RE, Chelikani P. 2010. Bitter taste receptor T2R1 is activated by dipeptides and tripeptides. Biochem Biophys Res Commun 398: 331-335.

Wong GT, Gannon KS, Margolskee RF. 1996. Transduction of bitter and sweet taste by gustducin. Nature 381: 796-800.

Wu SV, Chen MC, Rozengurt E. 2005. Genomic organization, expression, and function of bitter taste receptors (T2R) in mouse and rat. Physiol Genomics 22: 139-149.

Wu SV, Rozengurt N, Yang M, Young SH, Sinnett-Smith J, Rozengurt E. 2002. Expression of bitter taste receptors of the T2R family in the gastrointestinal tract and enteroendocrine STC-1 cells. Proc Natl Acad Sci U S A 99: 2392-2397.

Yan W, Sunavala G, Rosenzweig S, Dasso M, Brand JG, Spielman AI. 2001. Bitter taste transduced by PLC-beta(2)-dependent rise in IP(3) and alpha-gustducin-dependent fall in cyclic nucleotides. Am J Physiol Cell Physiol 280: C742-751.

Yang R, Crowley HH, Rock ME, Kinnamon JC. 2000. Taste cells with synapses in rat circumvallate papillae display SNAP-25-like immunoreactivity. J Comp Neurol 424: 205-215.

Zancanaro C, Sbarbati A, Bolner A, Accordini C, Piemonte G, Osculati F. 1995. Biogenic amines in the taste organ. Chem Senses 20: 329-335.

Zhang Y, Hoon MA, Chandrashekar J, Mueller KL, Cook B, Wu D, Zuker CS, Ryba NJ. 2003. Coding of sweet, bitter, and umami tastes: different receptor cells sharing similar signaling pathways. Cell 112: 293-301.